Molecular orientations in an extruded collagenous composite, the marginal rib of the egg capsule of the dogfish *Scyliorhinus canicula*; a novel lyotropic liquid crystalline arrangement and its origin in the spinnerets

D. P. KNIGHT[1], X. W. HU[1], L. J. GATHERCOLE[2], M. RUSAOUËN-INNOCENT[3], M.-W. HO[4] AND R. NEWTON[4]

[1] *Biosciences Group, King Alfred's College, Sparkford Road, Winchester SO22 4NR, U.K.*
[2] *H. H. Wills Physics Laboratory, University of Bristol, Bristol BS8 1TL, U.K.*
[3] *Laboratoire d'Histologie et Cytologie des Invertébrés Marins, Université P. et M. Curie, 12 Rue Cuvier, 75005 Paris, France*
[4] *Department of Biology, Open University, Walton Hall, Milton Keynes, MK7 6AA, U.K.*

SUMMARY

The egg case of the dogfish, *Scyliorhinus canicula* is a composite material largely constructed from collagen fibrils. It is formed as a drawn extrusion from transverse rows of spinnerets within the lining of the nidamental gland. In the L_2 layer, which forms over 90% of the thickness of the marginal rib, each spinneret extrudes a flattened ribbon which runs the length of the rib and measures approximately 150×8.5 μm in cross section. The structure of these ribbons and the orientation of collagen molecules and fibrils within them has been investigated in a correlative study using: low angle x-ray diffraction; bright field microscopy of peeled preparations; transmission (TEM) and scanning (SEM) electron microscopy; confocal and quantitative polarizing microscopy. The way in which the molecular orientations are defined within the spinneret has been followed by SEM of fixed material from actively secreting nidamental glands. The extruded ribbon showed a predominantly biaxial fibril orientation in low angle x-ray diffraction patterns recorded with the beam passing horizontally through the marginal rib. This x-ray pattern is derived from a remarkably regular parabolic arrangement of fibrils superficially resembling that seen in biological twisted nematic liquid crystals. However, evidence is presented here that the arrangement in the marginal rib is novel, apparently arising from authentically curved fibres showing a splayed- or bent- rather than twisted-nematic construction. Evidence is also presented that the spinnerets are able to control molecular orientations in a nematic liquid crystal to produce this and the other arrangements seen in the egg case.

1. INTRODUCTION

Collagenous composite materials are widespread throughout the animal kingdom, forming a wide range of structures including worm cuticles, connective tissues and coatings of cysts and eggs. Medically important collagenous composites include tendon, bone, dentine, dermis, cartilage, cornea and basement membrane. The fibril arrangement of these materials is often surprisingly complex showing order at several different hierarchical levels of organization (Lakes 1993). The orientation of collagen molecules and fibrils within these materials is a major determinant of their mechanical properties (Vincent *et al.* 1992; Hepworth *et al.* 1994). How fibril orientations are defined in collagenous composite materials and modified is a question of considerable interest with implications for the study of function, development, health, and disease. The dogfish egg case and the nidamental gland which secretes it provides a useful system for studying this question (Feng & Knight 1994*a*, *b*; Knight & Feng 1992, 1994). The egg capsule and associated tendrils show precise and complex patterns of fibril orientation yet these are defined by spinnerets of a remarkably simple construction, described elsewhere (Knight & Feng 1992; Feng & Knight 1994*a*; Knight *et al.* 1996). The capsule and tendril are both constructed from approximately 30 lamellae, each extruded from its own transverse groove within the inner lining of the nidamental gland. Each transverse groove contains a single row of spinnerets. Each spinneret is supplied by a short secretory duct which opens between two remarkable, plate-like folds of epithelium we have termed 'baffle plates' (Knight & Feng 1992). The spinnerets serve to orientate unaggregated molecules or small, possibly tetrameric oligomers, fibril formation

Phil. Trans. R. Soc. Lond. B (1996) **351**, 1205–1222
Printed in Great Britain

taking place later in the secretory pathway after the molecular orientations have been defined (Knight *et al.* 1996).

Evidence is presented that the flattened ribbon-shaped filament extruded from each spinneret is constructed from fibrils arranged in parabolically curved fibres. This arrangement is different from the parabolic one seen in a number of other structural materials (Bouligand *et al.* 1972, 1978, 1985). Variation in the pattern of fibril orientation from region to region in the egg case and associated structures suggests that the nidamental gland is able to control the parameters of lyotropic liquid crystalline assembly with remarkable precision.

2. MATERIALS AND METHODS

(*a*) *General methods*

Egg capsules of the dogfish, *Scyliorhinus canicula* were collected from aquarium tanks in the Portsea Sea Life Centre. Live sexually mature females of the same species were caught either by line-fishing off Portsmouth or by trawling in Weymouth Bay. The anatomical axes of the egg capsule are easily recognized and are referred to here as those of the female fish in which the capsule has a constant orientation, with the eclosion slit always at the anterior end.

The nomenclature used to describe the layers of the egg capsule is that of Rusaouën *et al.* (1976). All observations and figures in this paper refer, except where stated, to ribbons from the layer L_2 of the marginal rib.

The following definitions apply throughout this paper. Fibril, a unit of assembly in which all the molecules form a single coherent crystallite; fibre, a bundle of coaxially oriented fibrils; sheet or lamina, a planar structure formed from uniaxial or curved coaxial fibrils, many of which show accurate side-to-side registration of their axial banding pattern; lamella, a planar structure extruded from a single transverse groove in the nidamental gland. In the marginal rib, each lamella is constructed from a single row of ribbons. A nematic liquid crystal is one in which the molecules lie parallel or approximately parallel to one another, but without positional order. A wall effect, also known as a boundary effect, is an alignment of molecules of a nematic liquid crystal at the wall of a container. This alignment is usually parallel or perpendicular to the wall or boundary. Both twisted and splayed nematics can be considered to arise as modifications of a parallel wall effect. In the case of a twisted nematic, the molecules remain in a plane parallel to the wall but with increasing distance from it, their long axes progressively rotate in the plane of the wall. In a splayed nematic the molecules adjacent to the wall also lie in a plane parallel to it, but the progressive rotation is about axes in a plane perpendicular to the wall to give a curved arrangement. In a bent nematic, a curved arrangement is produced by a progressive rotation about axes parallel to the wall as in a splayed nematic but the molecules at the surface of the wall lie normal rather than parallel to it.

Standard deviations of measurements reported here are for $n > 10$ except where stated. The least squares method (Cricketgraph; Unistat 3 and Statistica) was used for curve fitting. To fit curves to micrographs of curved fibres, the coordinates of approximately 20 equally spaced points were entered after overlaying enlarged micrographs with transparent graph paper.

(*b*) *Low angle x-ray diffraction*

The methods have been described in detail elsewhere (Gathercole *et al.* 1993; Hepworth *et al.* 1994). Briefly, an Elliott GX21 generator and a Rigaku-Denki small angle camera were used with the x-ray beam collimated by 500 μm and 300 μm pinholes. Patterns were obtained by directing the beam perpendicularly through the full thickness of the marginal rib in two directions (as shown in figure 1): (i) along the major axis of the ellipse formed by the capsule in transverse section, the horizontal axis of the egg capsule; and (ii) along the minor axis of this ellipse, the vertical axis of the capsule. Specimens were maintained at 100% humidity in sealed Lindemann tubes.

(*c*) *Cryostat sections and peel preparations*

Cryostat sections 12–20 μm thick of unfixed marginal rib were cut in planes normal to the marginal rib at different angles (0°, 15°, 75° and 90°) to its long axis and mounted unstained in Aquamount (Merck Ltd.; refractive index 1.38). The plane of sectioning was defined by eye with the aid of a protractor. Planes at 15° and 75° to the long axis of the marginal rib were selected respectively to cut parallel and at right angles to the predominant molecular orientations in the marginal rib as determined by low angle x-ray diffraction (see below). Vertical longitudinal sections were also examined. To keep track of the antero-posterior axis of sections and of peels (see below) an anterior corner was cut off the edge of the tissue block before sectioning or peeling.

Thin layers peeled from marginal ribs as described elsewhere (Hepworth *et al.* 1994), were mounted flat in Aquamount or, after dehydration and clearing, in DPX. They were examined with polarizing and Nomarski microscopes. Some were examined by polarizing and brightfield microscopy after staining with picro-Sirius B red (Junqueira *et al.* 1980).

(*d*) *Polarizing microscopy*

Two methods were used to determine the patterns of orientation of the slow axes in unstained cryostat sections of fully formed marginal ribs.

1. A conventional polarizing microscope fitted with a first order red compensator was used to examine molecular orientations. A drawing was first made of a small region under investigation. The drawing was then rotated with the specimen and the slow axes in different regions were noted on it after observing how areas coloured intensely blue changed with specimen rotation.

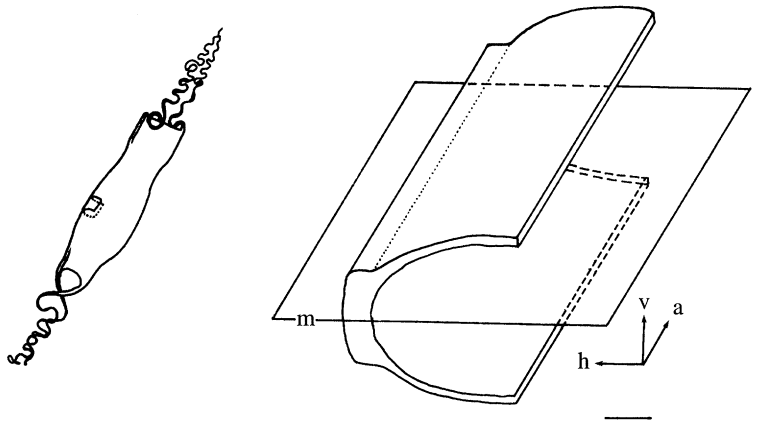

Figure 1. Diagram showing on the left, a whole egg capsule and on the right, an enlarged region to show the anatomical planes of the marginal rib (see text). Midline (m); horizontal (h); vertical (v); anterior (a). Scale bar 1 mm.

2. We also used a quantitative polarizing microscope fitted with a colour video camera directly interfaced to a microcomputer (provisional patent GB2270774A). The first order red plate was set at a small horizontal angle of rotation (7.5°) to the axis of the polarizer to produce more saturated interference colours compared with the conventional angle of 45° (Ho & Lawrence 1993; Ho & Saunders 1994, Newton *et al.* 1995*a*). Image analysis ('Nice Imaging' developed by Ross Research, Amersham, U.K. as an extension of Optimas, Data Cell) was used to measure and plot the intensity of the red signal at up to 100 points along a transect line across the specimen while the specimen was rotated stepwise, 5° at a time. The intensity of the red signal was used to calculate and plot the retardation and the angle of inclination of the slow axis to the transect line at each point along the transect. Theoretical curves (see the appendix) were fitted to selected parts of EXCEL files of retardation and angle plots using the least squares method (Statistica v 2.0). The slow axis in fibrillar collagens is parallel to the fibril axis (Bennet 1950).

Paraffin sections of an actively secreting nidamental gland fixed as described below were used to study molecular orientations in secreted material in different parts of the secretory pathway.

(*e*) *Confocal microscope*

A Leica TCS 4D laser scanning confocal microscope with an air-cooled, mixed gas (Krypton/Argon) laser light source was used. Auto-fluorescence was demonstrated using epi-illumination at an excitation wavelength of 488 nm (emission wavelength of 520 nm). A pin-hole setting of 30 was used to maximize resolution obtainable with a X25 oil immersion objective (NA 0.75). A series of 15 confocal 'optical slices' were scanned through a selected area of the total thickness of the specimen, each 'slice' measuring 0.33 μm in thickness. Selected images were then displayed on a high resolution, flat field monitor screen using a variety of computer generated colours.

Birefringence was demonstrated using conventional (non-confocal) transmitted light polarizing optics with a 488 nm laser light source. Objective magnification, step size, area scanned and number of 'optical slices' taken were identical to those used for the demonstration of the autofluorescence. Selected autofluorescent and polarized images were then superimposed on the monitor screen and photographed.

(*f*) *Scanning and transmission electron microscopy*

Methods for scanning (SEM) and transmission electron microscopy (TEM) have been described elsewhere (Knight & Feng 1992; Knight *et al.* 1993). Briefly, four types of preparation were examined by SEM.

1. Three actively secreting nidamental glands were fixed by perfusion in a modified Karnovsky fixative. After further fixation by immersion in the same fixative, natural casts formed from the fixed secretory material within the secretory tubules, spinnerets and transverse grooves were gently pulled from the tendril/marginal rib forming region. Whole mounts of natural casts mounted in glycerol were also examined by polarizing microscopy.

2. Thick transverse and longitudinal slices of three fully formed marginal ribs and transverse slices of one marginal rib fixed *in situ* during formation were cut, unfrozen, with new razor blades from fixed tissue.

3. Pieces of marginal rib were infiltrated with DMSO, frozen in liquid nitrogen and fractured as described in Knight & Feng (1994).

4. Pieces of marginal rib from which peels had been removed as described above were fixed in osmic acid solution, and mounted on a stub before drying. All material was critical point dried, sputter coated and examined in the SEM.

For TEM, material was fixed in a modified Karnovsky fixative and post-fixed in Dalton's osmium tetroxide solution before dehydration and embedding in Spurr's resin. Thick and ultrathin sections were cut from fully formed marginal ribs after embedding. Vertical longitudinal (VLS), horizontal longitudinal (HLS) and transverse sections (TS) were examined. VLS's were cut from

the marginal rib forming region in an actively secreting nidamental gland.

3. RESULTS

(*a*) *Low angle x-ray diffraction*

Figure 3 shows the pattern obtained by directing the beam along the major axis of the ellipse seen in transverse section of the whole capsule, through the full thickness of a rectangular rod specimen of marginal rib. There appeared to be two off-meridional series of reflexions separated by an angle of approximately 29°, equivalent to an angle of 14.5° to the long axis. This strongly suggests that in the central region of the marginal rib there are only two predominant orientations. As there is no axial offset between the two sets of reflections, we can be confident the effect does not arise from a sequential zig-zagging of continuous units (Gathercole & Keller 1991), but is almost certainly due to singly oriented units overlying each other at around 14.5°. All eleven reflexions are indexable as orders 1 to 11 of a mean repeat of 40.2 nm, and are closely comparable to the repeats of 39.4 nm and 40.4 nm recorded for main capsule wall material (Gathercole *et al.* 1993; Hepworth *et al.*1994).

The equatorial arcing is of the same angular magnitude at least as the meridional and the two major diffuse, off-equatorial reflexions at 11.8 nm (compare 11.1 and 11.5 nm for the comparable reflexions in from the capsule wall; see Gathercole *et al.* 1993). This confirms the molecular identity of the marginal rib material with that forming the bulk of the capsule wall.

The interpretation of figure 3 is further strengthened by examining figure 4, a near-tangential diffraction pattern obtained with the beam directed along the minor axis of the ellipse, at an angle of approximately 90° to that in figure 1, but still perpendicular to the long axis of the capsule. The pattern closely resembles that in figure 2*c* of Gathercole *et al.* (1993). The latter pattern was obtained by directing the x-ray beam parallel to the long axis of the capsule through a full thickness slice of mid-capsule wall. We now see a similar pattern by directing the beam perpendicular to the long axis, in the region of the marginal rib. This suggests that the whole structure has been tilted or rotated by approximately a right angle. This can be understood in the light of the orientational changes revealed by light and electron microscopy in the midline of the marginal rib (see figure 10). If we examine figure 3, the meridian is considerably streaked, but any split is now under 14°; similarly the equatorial split is 12° maximum, as measured from the films. This is consistent with viewing the crossing angle of 15° reduced by projection. In a perfectly oriented tangential view of units crossing at 15°, we might expect the split to be reduced to zero, but this is unlikely to be obtainable. Microscopical study of transverse sections taken in the region of the marginal rib used for diffraction show that there is some folding of the lamellae (see below). This will result in variation in the angle the diffracting units, described below as ribbons, make to the x-ray beam. As this variation occurs with depth as well as position along and across the marginal rib, further collimation of the beam, a cylinder of 0.3 mm diameter, or use of accurate goniometer mounting are unlikely to yield better oriented patterns.

(*b*) *Light microscopy of peels*

Two types of patterns described below in detail were commonly seen in thin sheets of material peeled from the layer L_2 of the marginal rib: (i) a criss-cross pattern (figure 5); and (ii) a series of overlapping, nested parabolae (figures 6 and 7). Both patterns are thought to represent two different projections of the same structure resulting from fracture along different planes (see figures 2*a* and *b*) during preparation of the peel.

1. The criss-cross pattern appeared superficially to be derived from biaxially oriented fibres arranged in partially overlapping ribbons (mean width approximately 150 μm) which ran exactly longitudinally down the marginal rib (figure 6). The fibrils were arranged predominantly at approximately +9° and −9° to the long axis of the marginal rib (figure 5), crossing each other at a mean angle of $17.7 \pm 4.2°$. In agreement with the low angle x-ray diffraction data, through focusing revealed that the ribbons appeared to be inclined at a small angle to the plane of the peeled layer, overlapping like tiles on a roof. On close inspection, the pattern was not strictly biaxial, but appeared to be constructed from two sets of slightly curving fibres within each ribbon. The fibres ran nearly straight for much of their length but curved away from each other at their posterior ends (figure 5). The partial overlap of this arrangement resulted in an appearance resembling rows of fir trees with curving branches, the tops of the trees always pointing anteriorly along the marginal rib (figure 5). Much of the material close to the midline of the marginal rib showed this pattern.

2. The pattern of nested parabolic curves (figures 6 and 7) was occasionally seen close to the midline of the marginal rib but was much more frequent at the dorsal and ventral edges of the peel where the laminae were arranged at a greater angle to the vertical axis. This appearance and distribution can be explained by reference to figures 2*a*,*b* and figure 10. Close to the midline of the rib, the fracture plane of the peel probably ran mainly along the more or less vertical lamellae to produce the criss-cross pattern (figure 2*a*). Where the lamellae curved out of the vertical plane at the dorsal and ventral edges of the rib, the plane of fracture probably deflected to run parallel to the ribbon's x axis(figure 2*b*). Fracture along the latter plane is thought to produce the nested parabolic curve pattern and this is confirmed by SEM (see below). Many of the curves appeared to be true parabolae. The model $y = Ax^2 + Bx + C$ showed a close fit with coefficients all better than 0.96 for five fitted curves taken from the ribbon shown in figure 6. The mean value of the constant A for these curves was 0.036 ± 0.006; $n = 5$. Some curves turned slightly away from the fitted parabolae where the x axis met the edge of the ribbon. There was little difference in the shape of the parabolae in a given ribbon but some variation from ribbon to

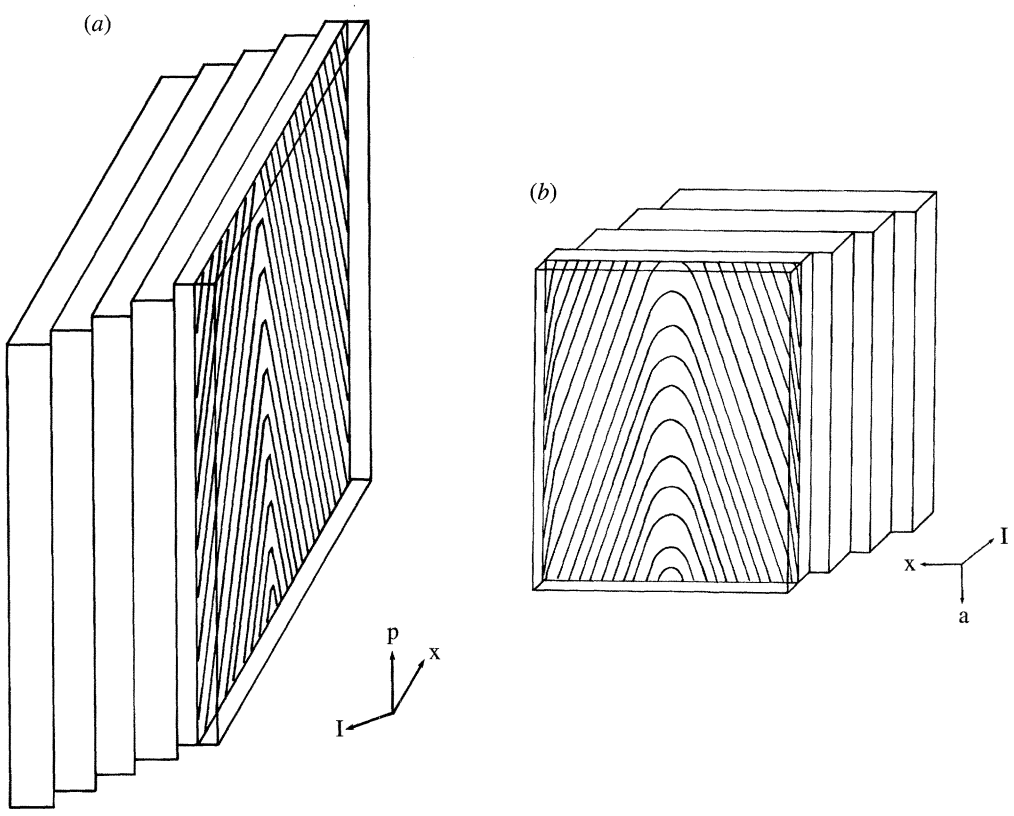

Figure 2. Semidiagramatic isometric drawings showing two views 90 ° apart of a small part of several ribbons within a single lamella. The shape of the lamella was derived from confocal observations. The nested parabolic pattern of molecular orientations is illustrated in a single sheet within a single ribbon. The plane of the lamella (I) is approximately vertical with respect to the egg case for lamellae close to the midline of the rib. The *x* axis of the parabolae (x) corresponds to that of the ribbon. (*a*) Shows how the predominantly biaxial pattern seen in peels and x-ray diffraction patterns is produced by fracture along the lamella. (*b*) Shows how the parabolic pattern in peels is produced by fracture along a plane parallel to the *x* axis of the ribbon. The parabolae point posteriorly (p); anterior direction (a). The width of the ribbon along its *x* axis measured approximately 150 μm

ribbon. The *y* axis of the parabolae lay parallel to the longitudinal axis of the marginal rib, the apogee always pointing towards the posterior end of the marginal rib.

Peels were used to study changes in the patterns in different regions. The curves became more rounded at the edges of the marginal rib. Similar rounded curves were seen in the outer lamellae of L_2 of the capsule wall proper (figure 8) but the lamellae of L_3 showed the orthogonal plywood pattern described elsewhere (Hepworth *et al.* 1994; Knight & Feng 1994).

(*c*) *Transmission electron microscopy*

Ultrathin sections revealed that the layer L_2 of the marginal rib appeared to be constructed largely from fibrils with transverse banding pattern, transverse crystalline lattice and D-period (figure 9) closely resembling those of the fibrils of the capsule wall proper described elsewhere (Wourms & Sheldon 1972; Knight & Hunt 1986). Each fibril appeared to be outlined by a very thin layer of relatively dense amorphous material probably representing matrix. The fibrils ran in bundles with their banding pattern in accurate registration for considerable distances (see figure 9). This lateral association between fibrils helps to explain why they form continuous sheets and probably relates to the relative lack of matrix in this material.

Ultrathin horizontal longitudinal sections of the marginal rib appeared to be constructed from lamellae. A parabolic fibril arrangement could be seen across the width of some of the lamellae, closely resembling the appearance seen in peels with the Nomarski microscope and the SEM. At the junction between two lamellae, in a position corresponding to the edges of the ribbon, the fibril orientation appeared to rotate rapidly in the plane of the *x* axis of the ribbon, in an opposite direction to the rotation observed in the middle of the ribbon. This rotation of fibrils joined the ends of the parabolic curves in adjacent ribbons smoothly together in a curve (figure 25). In transverse section, many ribbons showed a bundle of longitudinally sectioned fibrils at the midpoint of the ribbon, running parallel or nearly parallel to the *x* axis of this structure (figure 9 and 24). This bundle occupied the entire width of the ribbon at this point. At the ends of this bundle, the orientation of the fibrils appeared to change progressively and rather rapidly, the axis of the fibrils apparently rotating in the *x* plane of the ribbon. This resulted in rather sharp lines demarcating the ends of the longitudinally sectioned fibrils. These demarcation lines ran across the ribbon at angle of approximately 30° to the *x* axis.

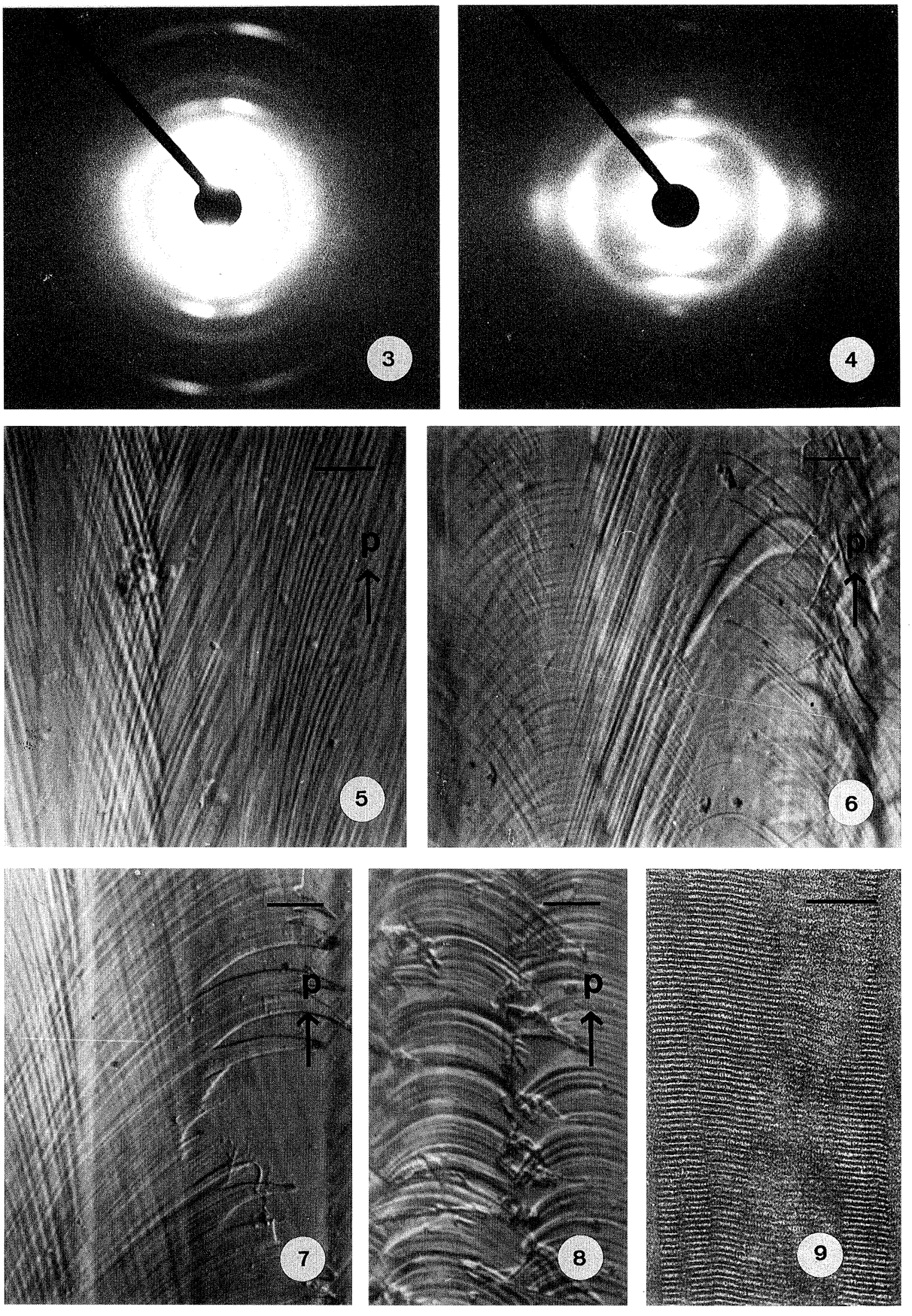

Figure 3. Low angle x-ray diffraction pattern recorded with the beam horizontal ±2° (figure 1). See text.

Figure 4. As figure 2 but with the beam vertical ±2°. See text.

Figure 5. Nomarski micrograph of a peel from a region of the marginal rib close to the midline. The material has a fibrous texture with a predominantly biaxial pattern crossing at about 17°. Careful examination shows that the fibres appear curved. Posterior (p). Scale bar 20 μm.

(*d*) *Bright field and confocal microscopy*

Transverse sections of the marginal rib revealed that the left and right marginal ribs were closely similar in appearance but each rib was asymmetric about the mid horizontal longitudinal plane of the egg capsule. This asymmetry results from the arrangement of tendril/marginal rib forming regions of the nidamental gland (Feng & Knight 1994*a*). The following description refers to the left marginal rib. The dorsal side was somewhat thicker, being composed of approximately 35 lamellae compared with approximately 25 on the ventral side. Compared to the lamellae of L_2 of the capsule wall proper, those of the equivalent layer of the marginal rib were considerably thicker. This, together with the difference in number of lamellae on the dorsal and ventral sides of the marginal ribs, appeared to produce some anticline-like tilting and folding of the lamellae (figure 10) not seen in the capsule wall proper. In some transverse sections of the marginal rib the folding was so pronounced at a single locus that a small number of ribbons appeared to have rotated relative to one another through an angle of more than 90° to produce a whorl. Despite this folding and whorl pattern, the majority of the lamellae in the midline were approximately tangential to the outer surface of the marginal rib.

The substructure of the L_2 lamellae of the dorsal and ventral sides of the marginal rib were similar in transverse section and were different from those of the egg capsule wall proper (Knight & Feng 1994) or the distal part of the tendrils (Feng & Knight 1994*a*). Each marginal rib lamella in transverse section appeared to be composed of a single row of longitudinally oriented ribbons packed closely together with little intervening material (figures 11–14). In longitudinal section the ribbons were seen to lie parallel to the long axis of the marginal rib, apparently running the whole length of the structure. The proximal parts of anterior and posterior tendrils showed a similar construction to the marginal rib.

In transverse sections the ribbons measured 148 ± 13 μm by 8.5 ± 1.2 μm, often appearing relatively straight but sometimes slightly curved into an S-shape or more complex curve (figures 12–14). The outline of relatively straight ribbons was often parallelogram-shaped in transverse section with the ends set at approximately 30° to the sides (figure 12). Whatever their shape, the ribbons were arranged like overlapping tiles set at an angle of approximately 30° to the plane of the lamella. The shape, dimensions, spacing and arrangement of the ribbons closely resembled that of the openings of the spinnerets within the transverse grooves (figure 16), strongly suggesting that each ribbon was derived as a continuous extrusion from a single spinneret. This was confirmed by examining vertical longitudinal paraffin and plastic sections of actively secreting nidamental glands. In these, a ribbon with its distinct pattern of orientations could be seen, fixed while emerging from each spinneret (see also Feng & Knight 1994*a*).

In transverse sections, the confocal microscope revealed that, in limited regions of the marginal rib close to the midline, each ribbon was outlined by a very thin layer of finely granular strongly autofluorescent material (figures 11–14). This localization suggested that the fluorescent material was secreted in, or immediately before the spinneret. Material outlining the ribbons could also be identified in SEM's of the transversely cut surface of the marginal rib (figure 17). The fluorescent outline of the ribbon provided a means of studying the shape, size and orientation of the ribbon and the location and orientation of birefringence within it (figures 11–14).

(*e*) *Scanning electron microscopy of the marginal rib*

SEM of peeled marginal ribs confirmed that a parabolic arrangement of fibres was seen when the fracture travelled in a plane parallel to the *x* axis of the ribbon (figures 2*b* and 21). It also confirmed that the criss-cross pattern described above was produced by the fracture running instead along the plane of the lamella (figure 2*a*). Peels and frozen fractured material revealed that each ribbon appeared to be composed of eight to ten thin sheets laid on top of each other and parallel to the *x* plane of the ribbon (figures 21–23). Each thin sheet had a rather constant thickness (0.5 μm) and appeared to be built up from nested, parabolic fibres. The parabolae in successive sheets within the ribbon appeared to be nearly exactly superimposed (figure 21) or were displaced by a small distance along the *x* axis (figure 22), the latter appearance compatible with the staggered model illustrated in figure 25. The parabolic arrangement of fibres was confirmed in frozen fractured material.

In transverse sections cut with a razor blade or fractured frozen, the profile of the cut surface of the

Figure 6. As figure 5 but showing nested parabolic curves. Posterior (p). Scale bar 20 μm.

Figure 7. As figure 5 but showing splitting between the curved fibres at the torn edge of a ribbon to the right of the micrograph. The torn sheet is evidently quite thin. This pattern of splitting is unlikely in a twisted nematic construction. Posterior direction (p). Scale bar 20 μm.

Figure 8. As figure 5 but showing a pattern of slightly overlapping parabolic curves seen in lamellae stripped from the outer lamellae of L_2 of the capsule wall proper. The parabolae are more rounded than those seen in figure 6. Posterior (p). Scale bar 50 μm.

Figure 9. Transverse ultrathin section of part of the central portion of a ribbon showing a number of fibrils running north/south across the micrograph and parallel to the *x* axis of the ribbon. The banding pattern appears closely similar to that of fibrils from the capsule wall proper and is in accurate lateral registration for much of the thickness of the bundle. Scale bar 200 nm.

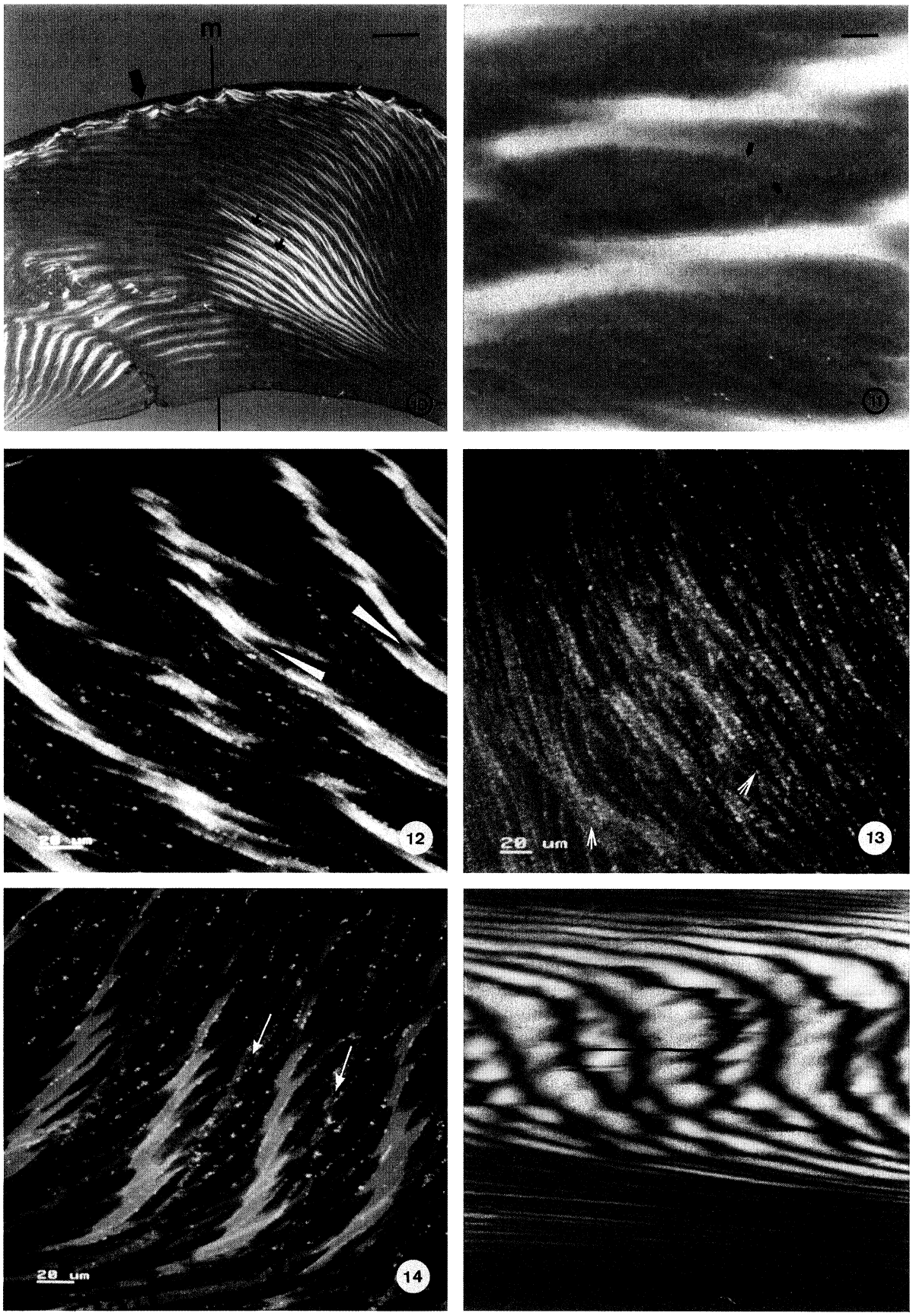

Figure 10. Polarizing micrograph of a transverse cryostat section of part of the marginal rib. The slow axis of the analyser ran from left to right. The first order red plate was set at an angle of 7.5° to this. The lamellae (narrow arrows) of layer L_2 are somewhat curved and can be seen to be constructed from rows of partly overlapping ribbons, the central parts of which are brightly and positively birefringent (blue interference colours to left and yellow to right of micrograph). Midline of the rib (m); outer surface (broad arrow). The outlines of the ribbons are not clearly demarcated in this figure. There approximate positions can be identified by reference to figure 12. Scale bar 200 μm.

ribbon varied systematically in different regions of the ribbon (figure 17). This is thought to represent a sectioning artefact in which the thickness of the section depends on the angle at which the fibrils were cut or fractured (see also Bouligand & Giraud-Guille 1985).

(*f*) *Polarizing microscopy*

Polarizing microscopy of the ribbons in different planes of section revealed a well-defined pattern of molecular orientations.

(i) *Longitudinal sections*

The progressive rotation of fibrils along the x axis of the ribbon (see below and figures 15 and 27) was confirmed by observing the effects of rotating vertical longitudinal sections on the stage of the polarizing microscope (see Neville 1993). This revealed sharp longitudinal bands of extinction within each lamella. Each band appeared to move across the lamella as the specimen was rotated. The movement of these bands was from left to right when the specimen was rotated anticlockwise through a small angle starting with its posterior axis pointing vertically on the cross-wires of the conventional polarizing microscope. This confirmed the observation from peel preparations that the apogee of the nested parabolae always pointed towards the posterior end of the marginal rib. A plot of the retardation along a transect across a ribbon showed a close fit ($R^2 = 0.988$) to the theoretical curve (eq. 7) derived in the appendix (see figure 27*b*). The plot of the angle of orientation for the same transect (figure 27c) also showed a fairly close fit ($R^2 = 0.930$) to the theoretical curve (eq. 6, in the appendix). The closeness of fit confirms the parabolic arrangement of fibrils within the ribbons. The values for the constant A of 0.011 and 0.020 derived from fitting curves respectively to the retardation and angle plots were in close agreement. These values were slightly less than the value (0.04) derived from fitting curves directly to the parabolae seen in peels (see figure 6). This slight difference may result from the fact that the plane of the longitudinal cryostat section is likely to be somewhat tilted relative to the x axis of the ribbon. This would result in an apparent narrowing of the parabola in sectioned material. The validity of the quantitative polarizing method was supported by the observation that the maximum retardation was always seen where the molecules were inclined at 90° to the transect line (figure 27*a*)

(ii) *Sections cut at 15° to the long axis*

These showed some resemblance to the longitudinal sections described above, the ribbons appearing markedly elongated. Some ribbons appeared to be sectioned in a plane nearly parallel to their x axes and at a small angle to the longitudinal. This had the effect of spreading out the pattern in two dimensions (figure 15). Transect lines parallel to the longitudinal axis across this pattern clearly showed a progressive change in molecular orientation (figure 28).

(iii) *Transverse sections*

In these, the central part of each ribbon was strongly birefringent and, in some regions, appeared to be constructed from parallel fibres (figure 12). The birefringence was markedly uniaxial with the slow axis parallel to that of the fibres (positive birefringence) and parallel to the x axis for most relatively straight ribbons (figures 12 and 29). The birefringence decreased rather rapidly at either end of this strongly

Figure 11. As figure 10 but at a greater magnification. The slow axis of the polarizer lay at −45° to the left to right axis of the figure. The ribbon can be seen to be outlined by tiny highly refractile granules (arrows). Only the central part of the ribbon (blue) appears strongly birefringent. This is because the y axis of the parabolae lie normal to the plane of section so that only fibrils at their apices lie parallel to the plane of section. Scale bar 10 μm

Figure 12. Cryostat section cut at 90° to the long axis of the marginal rib in a region similar to that appearing yellow in figure 10. Confocal autofluorescent image superimposed on non-confocal birefringent image; computer generated false colours. The slow axis of the analyser runs from left to right. The granular material outlining the ribbon (see figure 11) is autofluorescent (orange). The central part of each ribbon, representing the apex of the parabolic fibres, is positively birefringent (green or white depending on strength) and shows a fibrous texture in places (arrows). There is a sharp line demarcating the edge of the strongly birefringent portion and this is frequently parallel to the ends of the ribbon (see top third of micrograph). This observation is compatible with the staggered model shown in figure 25. Scale bar 20 μm

Figure 13. As figure 12 but cryostat section cut at approximately 75° to the long axis. Autofluorescence (green); birefringence (orange). Compared with figure 12, tilting the plane of sectioning has, as predicted, shifted the birefringent region to the end of each ribbon (arrows). Scale bar 20 μm

Figure 14. As figure 12 but cryostat section cut at approximately 85° to the long axis of the marginal rib and close to the edge of the autofluorescent area. Fluorescence (green); birefringence (orange). The ends of the ribbons (arrows) define the plane of the lamella. Material at the edge of the lamella lay adjacent to the wall of the transverse groove in the spinneret while material on the long faces of the ribbon lay adjacent to the baffle plates. This suggests that the fluorescent material is applied to the forming ribbon in or just before the spinneret. Scale bar 20 μm

Figure 15. Polarizing micrograph as figure 10 but section cut at approximately 15° to the long axis of the marginal rib. The upper edge of the section shows an alternation of thin, parallel laminae with molecules at +45° (blue), 0° (magenta), −45° (yellow) and 0° (magenta) as in a longitudinal section. Beneath this, curvature of the planes of the lamellae greatly broadens the pattern. Here the alternation in orientations can be clearly seen. Results from a transect along a line similar to that indicated are illustrated in figure 27. Transect line 400 μm

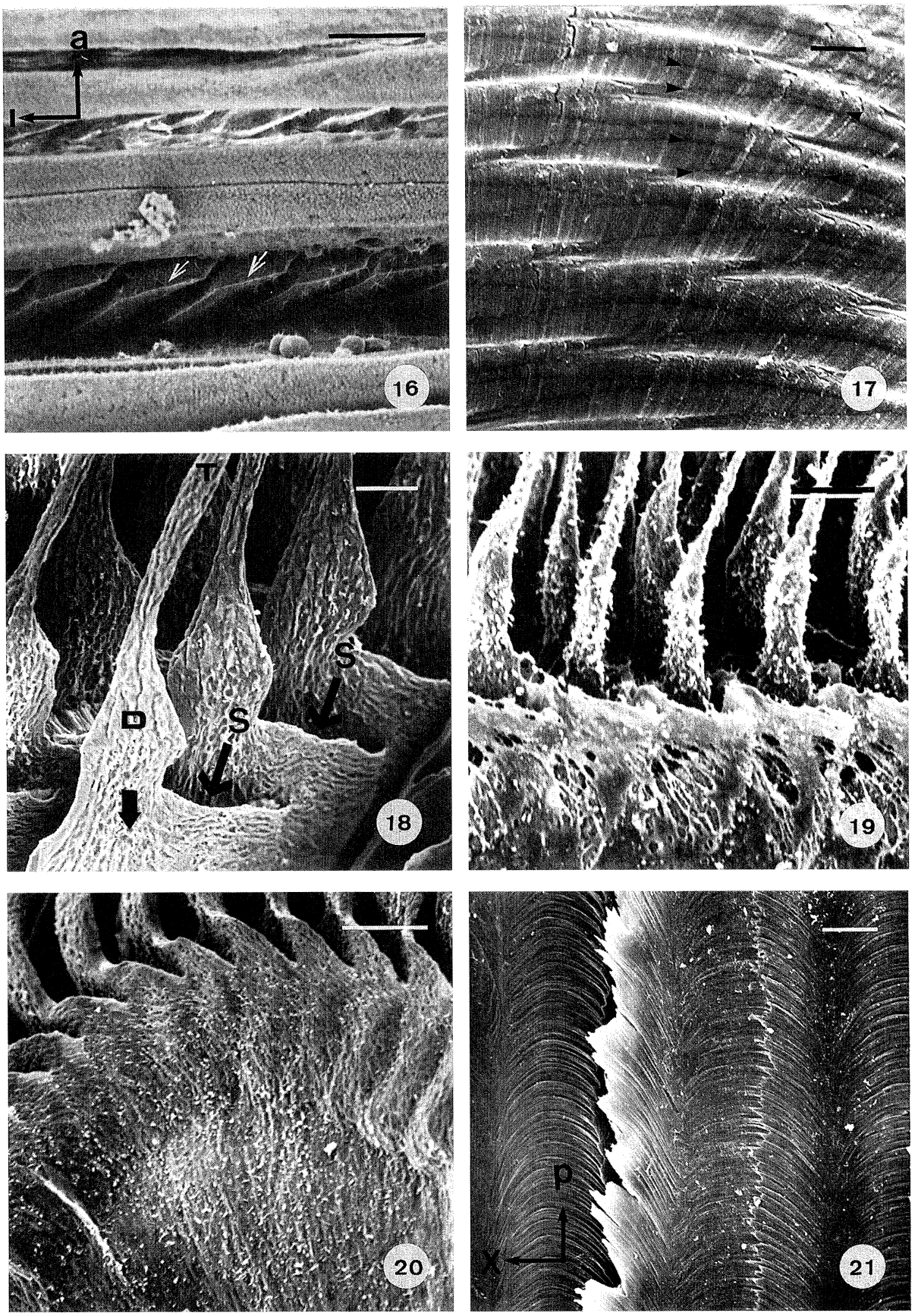

Figure 16. SEM looking down parts of two transverse grooves (running left to right) in the region of the nidamental gland which secretes the layer L_2 of the capsule wall proper. The baffle plates (arrowed) of the spinnerets can be seen overlapping and inclined at an angle of about 30° to the long axis of the groove. Compare with figure 17. Anterior (a); lateral (l). Scale bar 100 μm

birefringent patch to give sharp demarcation lines between the strongly and less birefringent material. These demarcation lines frequently ran across the ribbon at an angle of approximately 30° to the x axis, and parallel to the ends of the ribbon (figure 12). These observations are compatible with the suggestion that the y axis in successive thin sheets which make up a ribbon are slightly staggered along the ribbon's x axis (see above). The plot of the retardation along the x axis showed a maximum at the midpoint of the ribbon and decreased symmetrically on either side of this (figure 29). The region of maximum retardation is thought to correspond to the apogee of the parabola where the fibrils are cut exactly longitudinally in a transverse section (see figure 12). Again, there was a good fit ($R^2 = 0.866$) between the observed retardation curve and the theoretical expression (eq. 4; in the appendix). The value for the constant A of 0.023 derived from the expression for the fitted curve was in close agreement with the values determined in other ways (see above).

(iv) *Sections cut at 75° to the long axis*

The maximum retardation was shifted to one end of the ribbon's width (figure 13) as expected from the parabolic arrangement shown in figure 2*b*.

(*g*) *Formation of the ribbon and origin of molecular orientations within the spinneret*

Figures 18–20 and 30 show a narrow elongated thread of material (approximately 20 μm wide) secreted by the gland cells of the gland tubule fixed while flowing down the lumen of the tubule to the secretory duct. On reaching this structure, the flow widened out as it travelled through the short, somewhat flattened lumen of the secretory duct approximately 150 μm long and 90 μm wide at its widest point. From the secretory duct, the material entered the spinneret or extrusion die proper. Here material evidently flowed more or less radially into the flattened space between two flattened plate-like structures. The latter were arranged parallel to one another and at an angle of approximately 30° to the long axis of the base of the transverse groove in which they were situated (figure 16). Thus, material flowing slowly between a pair of plate-like structures leaves their apex as the flattened ribbon described above.

SEM study of natural casts (figures 18–20) also suggested how the fibrilar orientations may be defined during pulltrusion through the spinneret. Secretory material fixed as it flowed through the spinneret revealed a divergent pattern of fine elongated ridges (figures 18–20). This suggested that the pattern of fibres and ridges preserved in the cast may in some way relate to the molecular orientations in the secretory material as they are defined within the spinneret. Polarizing microscopy of whole mounted natural casts indicated how the parabolae develop as the material flows through the secretory duct and the space beween the baffle plates. These preparations also show that the ridges observed in the SEM lie at right angles to the molecular axes (figure 30). The apogee of the parabolic curves within the spinneret appeared to point in line with the direction of movement of the ribbon through the spinneret (figures 19–20).

3. DISCUSSION

(*a*) Lyotropic liquid crystallization and its application to the hierarchical structure of collagens

Before considering the origin of the molecular and fibrilar orientations in the marginal rib of the dogfish egg case it is necessary to discuss the nature of lyotropic liquid crystallization and its application to the hierarchical structure (Lakes 1993) of collagens generally. Evidence presented by Hukins & Woodhead-Galloway (1977, 1978) suggested that transversely banded collagen fibrils represent lamellar liquid crystals. We presented evidence that lyotropic liquid crystallization accounts for the formation of the

Figure 17. SEM of the cut surface of a transversely sectioned marginal rib. The similarity of the shape, size and orientation of the ribbons to the spinnerets which form them (figure 16) is remarkable. The ribbons appear outlined by a dark line (arrows) probably representing the autofluorescent material (compare with figures 12–14). The systematic changes in thickness probably represent an artefact caused by sectioning fibrils at different orientations. Scale bar 40 μm

Figure 18. SEM of a natural cast (see text) of spinnerets from the tendril/marginal rib forming region viewed from the posterior side. Secreted material is thought to flow down the lumen of the gland tubule (T) in a liquid crystalline state to pass through the secretory duct (D) into the space (S) between the baffle plates whose former position is indicated (arrow). The baffle plates were usually lost as the secreted material was pulled from the gland during specimen preparation. The surface of the material has a fibrous texture at right angles to the orientation of the collagen molecules within the material. Scale bar 50 μm

Figure 19. As figure 18. The development of a curving pattern of fibres (arrows) can be seen as the secreted material flows on further between the baffle plates. Posterior (P); Lateral (L). Scale bar 100 μm

Figure 20. As figure 18. The development of the curving pattern can be traced as the material flows on further apically through the transverse groove. The orientation of the material close to the wall of the transverse groove appears to be to be predominantly longitudinal. Scale bar 100 μm

Figure 21. SEM of peel preparation. The parabolic curves appear to be generated from curved fibres (arrows). Approximately half of a thin sheet appears to have been torn away from the central ribbon. This indicates that the ribbon is constructed from several layers of thin sheets laid on one another. In this case the parabolae in successive sheets appear to share the same y axis. Posterior (p); x axis of the ribbon (X). Scale bar 20 μm

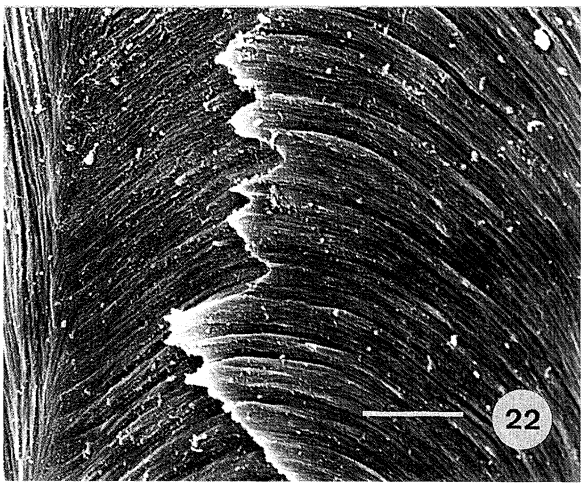

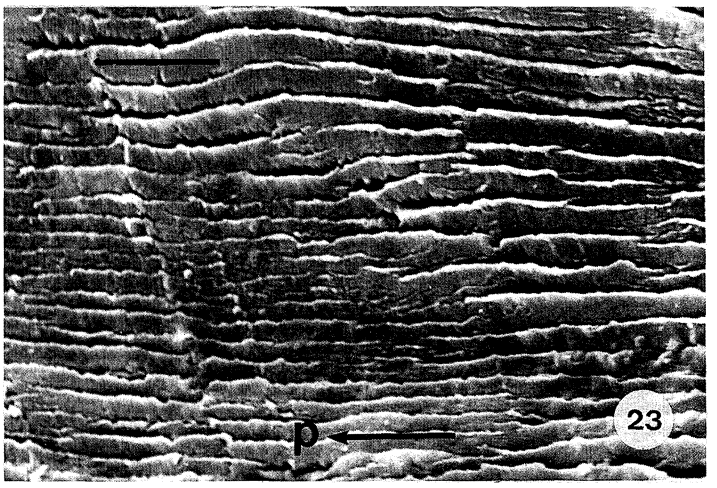

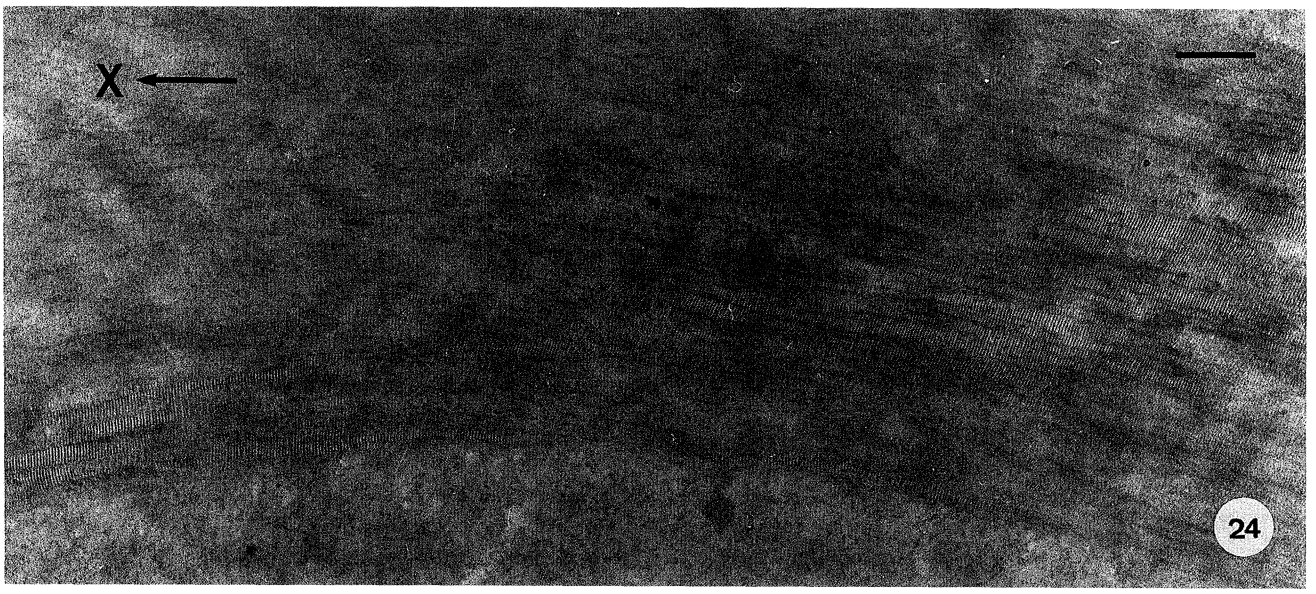

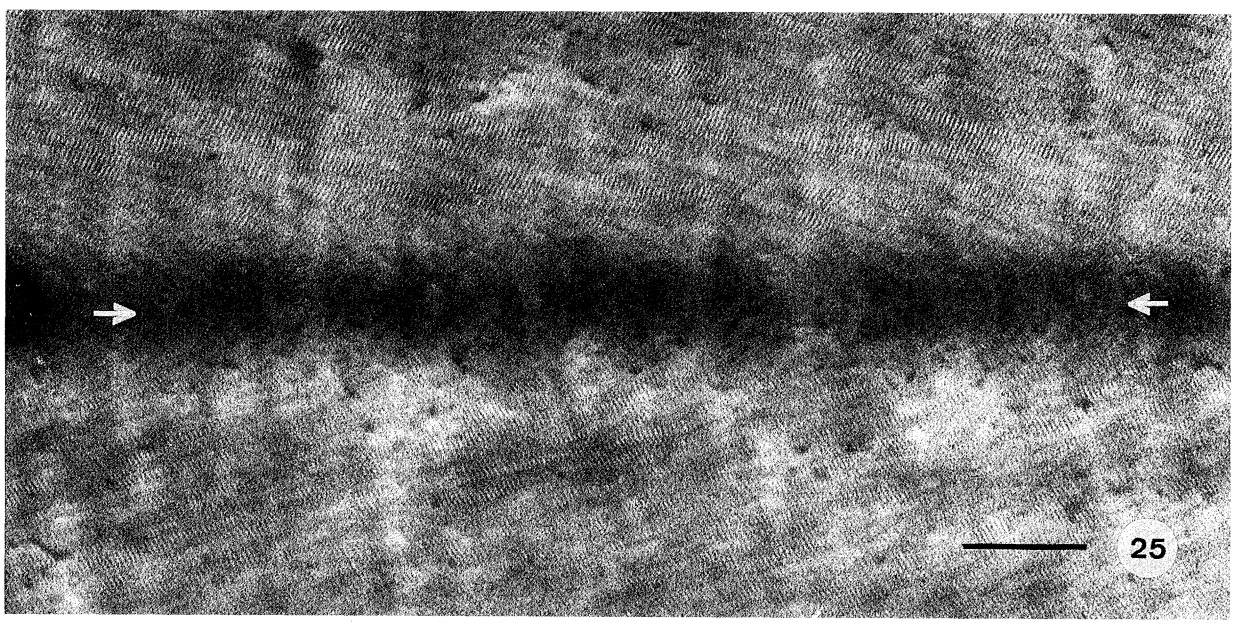

Figure 22. As figure 21. The ribbon can be clearly seen to be constructed from curved fibres laid in thin parallel sheets. The *y* axis of the parabolae appears to be slightly staggered in the two successive sheets. Scale bar 5 μm

Figure 23. SEM of part of a ribbon which appears to have fractured approximately longitudinally and approximately at right angles to the *x* axis. The ribbon appears to be constructed from numerous thin sheets. anteroposterior axis (p). Scale bar 4 μm

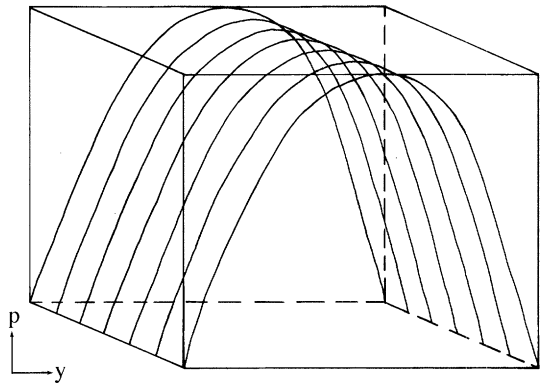

Figure 26. Simplified isometric diagram of the curved fibre model. For convenience, the thickness of the ribbon has been emphasized, the thickness of the fibrils have not been shown and only one set of parabolae have been drawn. The *y* axis of successive parabolae are staggered along the *x* axis of the ribbon as indicated by polarizing and TEM observations. *y* axis of ribbon (y); Posterior (p). The *x* axis of the ribbon measures approximately 150 μm.

collagen fibrils of the dogfish egg capsule (Knight & Feng 1994; Knight *et al.* 1996). A consideration of the nature of lyotropic liquid crystallization (Collings 1990) suggests that four prerequisites must be met before protein or other biological structural molecules can assemble in this way.

1. There must be a balance between attractive and repulsive forces between the molecules.

2. The molecules must be amphiphilic with a non-uniform axial distribution of hydrophobic side-chains. This is required for the formation of weak, reversible intermolecular interactions. In addition to hydrophobic interactions, electrovalent ones are also likely to be involved. An increase in entropy as water is disordered during formation of hydrophobic interactions and a decrease in enthalpy when charges are neutralized are probably important in fibril assembly. Thus the liquid crystalline assembly of collagen is an entropic process (Kadler *et al.* 1988).

3. The formation of intermolecular covalent or hydrogen bonds must be delayed until the molecules are in their final positions. The amphoteric nature of proteins may facilitate this, net charge on protein molecules providing sufficient repulsive force to prevent hydrogen bonding.

4. For some forms of liquid crystallization, the molecules must be non-racemic, that is present in a single chiral (handed) form.

There is evidence that dogfish egg case collagen meets each of these prerequisites (Knight & Feng 1994; Knight *et al.* 1996).

In addition to the assembly of the molecules into fibrils discussed in the previous paragraph, the fibrils in many collagenous tissues are in turn assembled into higher order structures (Lakes 1993). This process may also be essentially liquid crystalline (Besseau & Giraud-Guille 1995). The high axial ratio of the fully formed fibrils is unlikely to permit the freedom of rotation required for liquid crystalline assembly (Neville 1994*b*). The individual molecules, however, will have a much lower axial ratios and may be free to form ordered liquid crystalline assemblies on the surface of previously formed fibrils. Incorporation of these molecules into new fibrils without a change in molecular orientation would result in fibrilar orientations defined by liquid crystallization. In the example of dogfish egg case collagen, two considerations suggest that liquid crystallization is even more likely to be involved in the ordering of higher hierarchical levels. Firstly, the material is still fluid within the spinnerets, fibrils forming considerably later in the secretory pathway. Complex patterns of molecular orientations may thus be defined in the spinnerets by liquid crystallization and later locked in place by fibril formation and subsequent intermolecular cross-linking without drastic changes in molecular orientation (Knight *et al.* 1996). Secondly, the relative freedom of the dogfish egg case collagen molecules to rotate is likely to be enhanced by their very short molecular length (approximately 45 nm). It is worthy of note that even after extensive cross-linking, collagenous twisted nematic assemblies may retain a high degree of liquid-like mobility. This is suggested by the observation that interference colours generated by the lamellated construction of the scales of a teleost fish, change in solutions of different tonicity (Bone & Denton 1971). It seems likely that the lamellated construction of the scales, like those of the Coelacanth (see below), arises from twisted nematic assemblies of collagen and that changes in water content alter the pitch of the liquid crystal resulting in changing interference colours. The mobility of cross-linked collagenous assemblies is further supported by the observation that dogfish egg case fibrils (Knight & Feng 1994) and elastoidin spicules (Hukins *et al.* 1976*b*) appear to undergo a smectic A to smectic C transition when their water content is reduced.

(*b*) *Nature and origin of the parabolic pattern within the ribbons*

It is necessary to make a choice between a curved fibre model (figure 26) and a conventional twisted nematic model (figure 31) to account for the parabolic patterns described above. In the former, the parabolae result from actual, continuous, parabolic fibres (see illustration in Bouligand 1972). In the latter, the

Figure 24. TEM showing the central part of a ribbon seen in a transverse ultrathin section. The orientation of the fibrils here confirms the polarizing microscope observations. Successive collagen fibrils appear to rotate in the **x** plane (X) arrows. There is some evidence of a successive staggering of regions showing accurately longitudinally sectioned fibrils (see also figures 12, 22 and 26). Scale bar 500 nm

Figure 25. TEM of ultrathin HLS showing the rapid rotation of fibrils at the junction between two ribbons which appears as a dark line (arrows). The apogee of the tight parabolae formed in this way point anteriorly, in the opposite direction to the broader parabolae in the middle of the ribbon not seen in this figure. Scale bar 500 nm

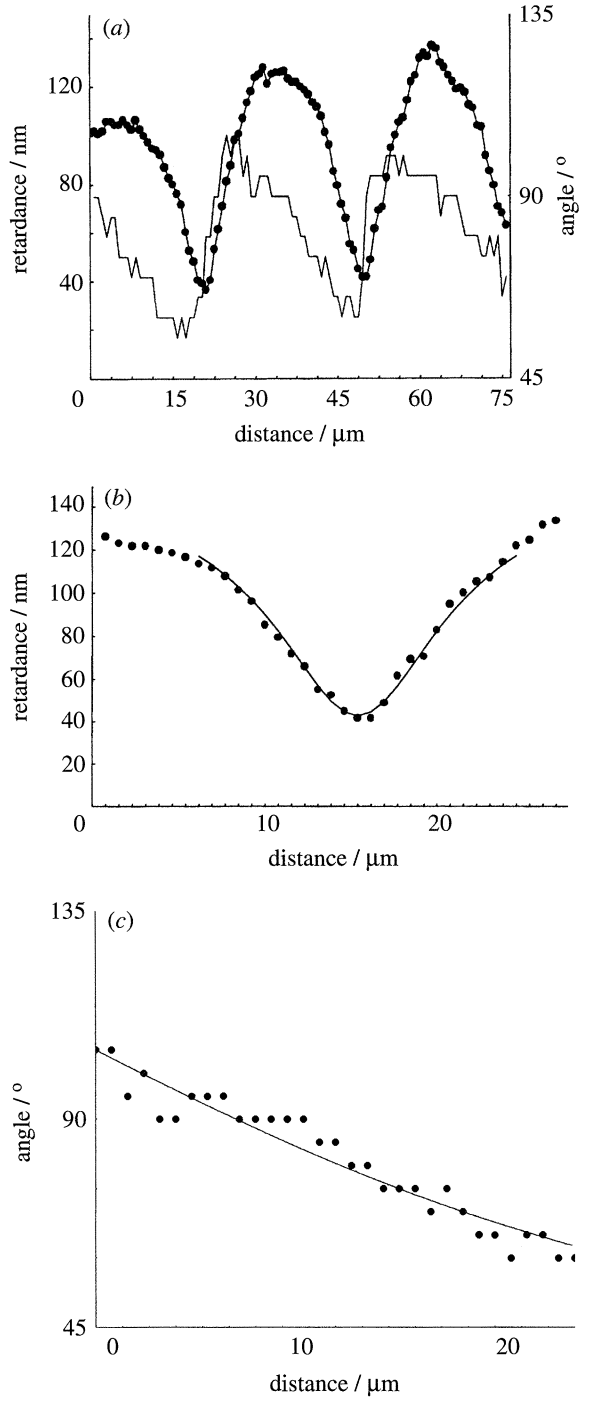

Figure 27 (*a*) Retardance and angle of inclination plots. Horizontal longitudinal section of marginal rib. Transect at 90° to the long axis of a ribbon; see text. Line with bullets denotes retardance (nm); line denotes angle of orientation. (*b*) and (*c*) show theoretical curves fitted to parts of the observed plots shown in part (*a*); see text and appendix 1. The equations for the fitted curves were as follows: (*b*) (retardation), $A = 44.\ \cos\ [\tan^{-1}(2.0 \times 0.011x)]$; $R^2 = 0.988$. (*c*) (angle of inclination), $A = \tan^{-1}(-2.0 \times 0.020x)$; $R^2 = 0.930$. The closeness of fit was not as good at the edges of the ribbon. This is compatible with the observation that the curves seen in peels sometimes bent away from a true parabola at the edge of the ribbon (see figure 25).

impression of parabolae arises as a sort of multilayered moiré effect from the superposition of successive sheets of fibrils in the following manner: Each sheet is

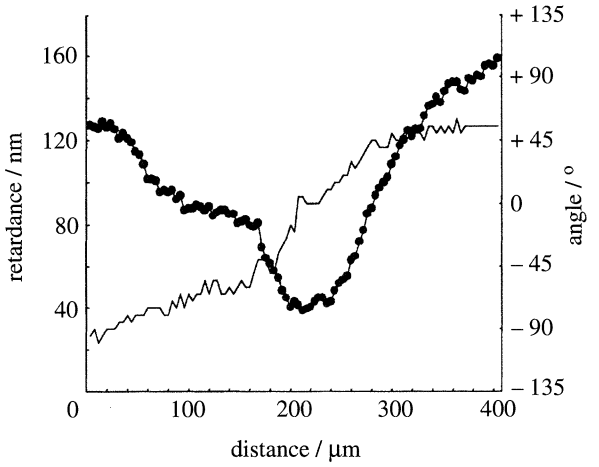

Figure 28. As figure 27*a* but for a nearly longitudinal section of marginal rib cut in a plane tilted through 15° to the horizontal axis. Transect line similar to the one shown in figure 15; See text. Line with bullets denotes retardance (nm); line denotes angle of orientation.

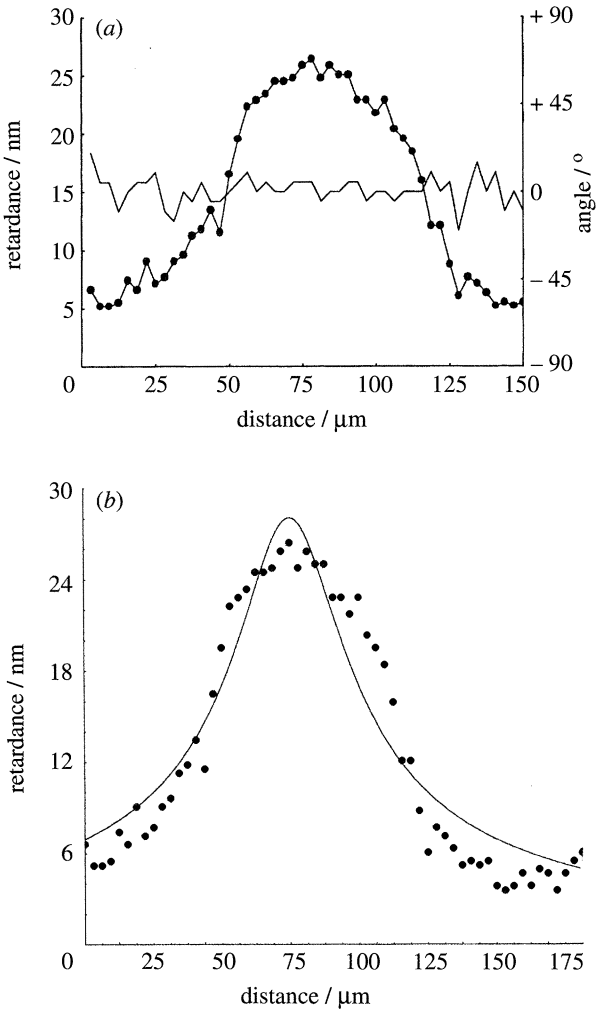

Figure 29 (*a*) As figure 27*a* but for a transverse section of ribbon. Transect line parallel to the x axis of a ribbon. See text. Line with bullets denotes retardance (nm); line denotes angle of orientation. (*b*) The theoretical curve $A = 27.4 \times \cos\ [\tan^{-1}(-2.0 \times 0.023x)]$ showed a fairly close fit ($R^2 = 0.866$) to part of the retardation plot shown in figure 28*a*. See text and appendix.

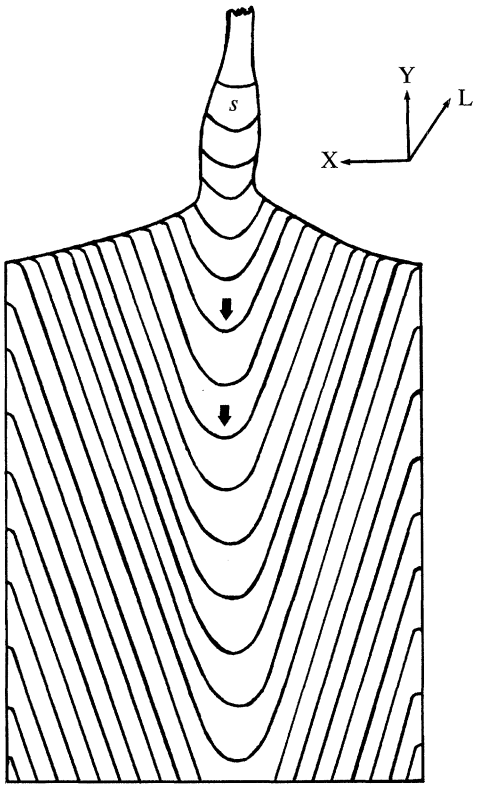

Figure 30. Isometric diagram showing how the pattern of molecular orientations is thought to develop as the material flows through a spinneret. Polarizing microscopy indicates that the parabolic molecular arrangement first develops as the material flows through the secretory duct (S). Direction of extrusion (arrows); *y* axis (Y); plane of the lamella (L). The *x* axis (X) of the ribbon is 150 μm long.

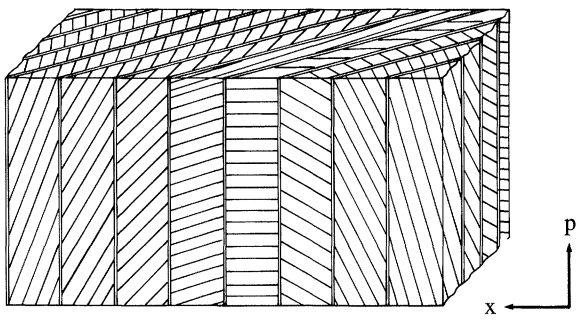

Figure 31. Isometric drawing of the twisted nematic model for the ribbon. For convenience only the central part of the ribbon has been drawn. *x* axis (x); Posterior (p).

constructed from fibrils lying parallel to each other and to the plane of the sheet. Successive sheets are laid on top of one another such that there is a progressive rotation of the fibril axis from sheet to sheet (Bouligand 1972). The two models are essentially rather similar at the molecular level; the axis of successive molecules rotating in both. In the fibre model successive fibrils along a fibre within a sheet undergo rotation. In this model, the fibrils close to the edges of the ribbon lie approximately parallel to the ribbon's long axis. This arrangement resembles that of a bent nematic (see above).

Four observations strongly favour the curved fibre model and rule out the twisted nematic one.

1. In the SEM, the parabolae can be seen in successive thin sheets laid one on top of each other and parallel to the *x* plane of the ribbon (figures 21–23). Such an appearance cannot be generated by a twisted nematic model. Cleavage along the sheets in the twisted nematic model should reveal uniaxially orientated sheets. These cannot be seen by light microscopy or SEM in peels prepared from the marginal rib.

2. The torn surfaces of peels sometimes showed curved splits running in the same direction as the curved lines of the parabolae (figure 7). This type of splitting should not occur in the twisted nematic model.

3. The individual parabolae in peels of marginal rib appeared to be quite thin, moving rapidly in and out of focus when through focusing. By contrast the parabolae in the twisted nematic model should be relatively insensitive to through focusing, giving similar appearances throughout the thickness of the ribbon.

4. The twisted nematic model can only account for a birefringent area in the middle of the ribbon in transverse section if the axis of the birefringence ran at an angle to the ribbon's *x* axis (figure 29). Observations with the polarizing microscope however indicated that the slow axis was generally parallel to the *x* axis of the ribbon (see above and figures 12 and 29).

The parabolic pattern described above in the marginal rib of the dogfish egg case shows a superficial similarity with that seen in synthetic twisted nematic liquid crystals and in a variety of biological structural materials (Bouligand *et al.* 1972, 1978, 1985; Neville 1978, 1993, 1994). Parabolic patterns, apparently with a twisted nematic organization, have been described in a range of other collagenous materials including Coelacanth scales (Giraud *et al.* 1978), bone osteons (Giraud-Guille 1988) and sonicated type I fibres (Giraud-Guille 1989). The analysis presented in the previous paragraph suggests however that the arrangement in the dogfish egg case marginal rib resembles that of a bent or splayed nematic rather than a twisted one. Does this resemblance represent mere analogy or are the molecular orientations actually defined by nematic liquid crystallization? Evidence reviewed above indicates that the material within the spinneret is fluid yet highly ordered and shows a similar pattern of molecular orientations to that in the final ribbon. This strongly suggests that the pattern is defined in the spinneret at least in part by liquid crystallization. It also suggests that the fibrils, when they form later in the secretory pathway evidently do so, without drastic molecular re-orientation. How could the curved patterns form in the spinneret? Bending can result from shear produced by flowing a nematic with a perpendicular wall effect through a capillary. Similarly, a splayed nematic arrangement can be produced where a magnetic field tends to rotate the molecules at right angles to the parallel alignment produced by the wall effect (de Gennes & Prost 1995). There is insufficient evidence to distinguish between

these two possibilities at present but neither arrangements appear to have been reported so far in biological materials.

The considerable width of the parabolae within the ribbons of the marginal rib and the continuity of the pattern across ribbons suggests that the dogfish is able to exploit lyotropic liquid crystallization to produce long range order. This may be of considerable general significance. The relatively large curved arcade pattern seen in cross-sections of articular cartilage (Clark 1985; de Bont *et al.* 1986) shows some similarity to the pattern described above. It is not impossible that this and other patterns with long range order in biological systems are dependent on lyotropic liquid crystallization.

(*c*) *Variation and control of the orientations extruded from the spinnerets*

It is instructive to compare the fibril arrangements in the marginal rib with those in other parts of the dogfish egg case and its associated tendrils. For example, the inner lamellae of the capsule wall proper (Layer L_3) have an orthogonal plywood construction while the outermost ones give parabolic patterns (Knight *et al.* 1996). This suggests a remarkable ability of the spinneret to control the orientations in the extruded material. This is further emphasized by the observation that the same spinnerets in the region which forms both tendril and marginal rib are apparently able to vary the pattern (Knight *et al.* 1996). They first produce a predominantly uniaxial, longitudinal arrangement seen in the distal part of the posterior tendril, then the parabolic arrangement described above in the marginal rib later returning to the uniaxial arrangement in the distal part of the anterior tendril. The apparent ability of the dogfish to control the orientation of nematic liquid crystals thus parallels the ability of other organisms to control the formation of true inorganic crystals (Albeck *et al.* 1993; Aizenberg *et al.* 1994).

We have traced the origins of the parabolic pattern back to the spinneret and suggested how the orientations change as the liquid collagen flows into it. It is not yet clear how the spinnerets and transverse grooves exert fine control over the process of liquid crystalline assembly to vary the pattern of orientations in the extruded ribbons from region to region. It is, however, likely that rheology of the liquid crystalline collagen is important, the relatively simple geometry of the spinneret helping to define the molecular orientations. The directional beating of cilia on both the plates and the walls of the transverse groove may play a part in this process (Knight & Feng 1992). The regional variation in the patterns produced by spinnerets may result from changes in the consistency of the extruded material. In this connection we have suggested that the epithelium of the transverse grooves absorbs water and hydrogen ions from the extruded material, controlling the viscosity and site of fibril formation (Feng & Knight 1994*b*). The rate of water removal and pH change may thus depend on the depth of the transverse grooves which varies systematically from place to place in the nidamental gland, the deepest grooves secreting the thickest and most complexly orientated lamellae. Precise regulation of pH and water content by the grooves may thus control the viscosity and phase transition of this lyotropic liquid crystalline material, altering its rheology and pattern of molecular orientation.

It is likely that the different patterns of orientation in different regions of the egg capsule and tendrils help define the sophisticated and regionally varied mechanical properties of this material (Hepworth *et al.* 1994; Knight *et al.* 1996). Thus the nidamental gland's ability to spin collagenous sheets and fibres with precisely defined yet regionally varied molecular orientations may offer considerable biomimetic potential.

We wish to thank Dian Feng for taking some of the micrographs; Martin Knight for help with the mathematical modelling; Moses Scott for catching the fish; the Sea Life Centre, Portsea for storing them for us; and the staff of the EM unit, Southampton General Hospital for help and advice. We gratefully acknowledge financial support from King Alfred's College (D. P. K.), from ORSAS (X. W. H.) and from an EPSRC-LINK grant (M-W. H.).

REFERENCES

Aizenberg, J., Albeck, S., Whiner, S. & Addadi, L. 1994 Crystal protein interactions studied by overgrowth of calcite on biogenic skeletal elements. *J. Cryst. Growth* **142**, 156–164.

Albeck, S., Aizenberg, J., Addadi, L. & Whiner, S. 1993 Interaction of various skeletal intracrystalline components with calcite crystals. *J. Am. Chem. Soc.* **115**, 11691–11697.

Bennet, H. S. 1950 The investigation of biological materials with polarized light. In *McClung's handbook of microscopical technique*, edn 3 (ed. R. McClung-Jones). New York: Paul B. Hoeber Inc.

Besseau, L. & M.-M. Giraud-Guille 1995 Stabilisation of fluid cholesteric phases of collagen to ordered matrices. *J. molec. Biol.* **251**, 197–202.

Bone, Q. & Denton, E. J. 1971 The osmotic effects of e. m. fixatives. *J. Cell Biol.* **49**, 571–581.

Bouligand, Y. 1972 Twisted fibrous arrangements in biological materials and cholesteric mesophases. *Tiss. Cell* **4**, 189–217.

Bouligand, Y. 1978 Cholesteric order. In *Biopolymers A. C. S. Symposium Series* vol. **74**, pp. 237–247.

Bouligand, Y., Denefle, J.-P., Lechaire, J.-P. & Maillard, M. 1985 Twisted architectures in cell-free assembled collagen gels: study of collagen substrates used for cultures. *Biol. Cell.* **54**, 143–162.

Bouligand, Y. & Giraud-Guille, M.-M. 1985 Spatial organization of collagen fibrils in skeletal tissues: analogies with liquid crystals. In *Biology of invertebrate and lower vertebrate collagens NATO ASI series A.* (ed. A. Bairati & R. Garrone) vol. **93**, pp. 115–134.

Clark, J. M. 1985 The organization of collagen in cryofractured rabbit articular cartilage: a scanning electron microscopic study. *J. Orthop. Res.* **3**, 17–29.

Collings, P. J. 1990 Liquid crystals: nature's delicate phase of matter. New Jersey and Oxford: Princeton University Press.

De Bont, L. G., Liem, R. S., Havinga, P., Boering, G. & van der Korst, J. 1986 Collagenous network in cartilage of human femoral condyles. A light microscopic and scanning electron microscopic study. *Acta Anat.* **126**, 41–47.

De Genes, P. G. & Prost, J. 1995 *The physics of liquid crystals*. Oxford: Clarendon Press.

Feng, D. & Knight, D. P. 1994*a* Structure and formation of the egg capsule tendrils in the dogfish *Scyliorhinus canicula*. *Phil. Trans. R. Soc. Lond.* B **343**, 285–302.

Feng, D. & Knight, D. P. 1994*b* The effect of pH on fibrillogenesis of collagen in the egg capsule of the dogfish, *Scyliorhinus canicula*. *Tiss. Cell* **26**, 649–659.

Gathercole, L. J., Atkins, E. D. T., Goldbeck-Wood, E. G. & Barnard, K. 1993 Molecular bending and networks in a basement membrane-like collagen: packing in dogfish egg capsule collagen. *Int. J. Biol. Macromol.* **15**, 81–88.

Gathercole, L. J. & Keller, A. 1991 Crimp morphology in the fibre-forming collagens. *Matrix* **11**, 214–234.

Giraud, M.-M., Castanet, J., Meunier, F. J. & Bouligand, Y. 1978 The fibrous structure of coelacanth scales: a twisted 'plywood'. *Tiss. Cell.* **10**, 671–686.

Giraud-Guille, M.-M. 1988 Twisted plywood architecture of collagen fibrils in human compact bone osteons. *Calcif. Tiss. Int.* **42**, 167–180.

Giraud-Guille, M.-M. 1989 Liquid crystalline phases of sonicated Type I collagen. *Biol. Cell.* **67**, 97–101.

Hepworth, D. G., Gathercole, L. J., Knight, D. P., Feng, D. & Vincent, J. F. V. 1994 Correlation of ultrastructure and tensile properties of a collagenous composite material, the egg capsule of the dogfish, *Scyliorhinus spp.* a sophisticated collagenous material. *J. struct. biol.* **112,** 231–240.

Ho, M. W. & Lawrence, M. 1993 Noninvasive interference colour imaging. *Microscopy and Analysis*, **September**, p. 26.

Ho, M. W. & Saunders, P. T. 1994 Liquid crystalline mesophases in living organisms. In *Bioelectrodynamics and Biocommunication* (ed. M. W. Ho, F. A. Popp & V. Warnke). Singapore: World Scientific.

Hukins, D. W. L., Woodhead-Galloway, J. & Knight, D. P. 1976 Molecular tilting in dried elastoidin and its implications for the structures of other collagen fibrils. *Biochem. Biophys. Res. Commun.* **73**, 1049–1055.

Hukins, D. W. L. & Woodhead-Galloway, J. 1977 Collagen fibrils as examples of smectic A biological fibres. *Molec. Cryst. Liq. Cryst. Lett.* **41**, 33–39.

Hukins, D. W. L. & Woodhead-Galloway, J. 1978 Liquid crystal model for the organization of molecules in collagen fibrils. *Biochem. Soc. Trans.* **6**, 238–239.

Junquiera, L. C., Bignolas, G., Mourao, P. A. & Bonetti, S. S. 1980 Quantitation of collagen-proteoglycan interaction in tissue sections. *Con. Tiss. Res.* **7**, 91–96.

Kadler, K. E., Hojima, Y. & Prockop, D. J. 1988 Assembly of type I collagen fibrils *de novo*. *J. biol. Chem.* **263**, 10517–10523.

Knight, D. P. & Feng, D. 1992 Formation of the dogfish egg capsule; a coextruded, multilayer laminate. *J. Biomimet.* **1**, 151–175.

Knight, D. P. & Feng, D. 1994 Some observations on the collagen fibrils of the egg capsule of the dogfish, *Scyliorhinus canicula*. *Tiss. Cell* **26**. 385–401.

Knight, D. P., Feng, D., Stewart, M. & King, E. 1993 Changes in macromolecular organization in collagen assemblies during secretion in the nidamental gland and formation of the egg capsule wall in the dogfish *Scyliorhinus canicula*. *Phil. Trans. R. Soc.* B **341**, 419–436.

Knight, D. P., Feng, D. & Stewart, M. 1996 Structure and function of the selachian egg case. *Biol. Rev.* **71**, 81–111.

Knight, D. P. & Hunt, S. 1986 A kinked molecular model for the collagen-containing fibrils in the egg case of the dogfish *Scyliorhinus canicula*. *Tiss. Cell* **18**, 201–208.

Lakes, R. 1993 Materials with structural hierarchy. *Nature, Lond.* **361**, 511–515.

Neville, A. C. 1978 *Biology of the arthropod cuticle*. U.S.A: Carolina Biological Supply Company.

Neville, A. C. 1993 *Biology of fibrous composites: development beyond the cell membrane*. Cambridge University Press.

Neville, A. C. 1994 Twisted nematic liquid crystals in biology. *Chemistry & Industry*, **March Edition**, pp. 176–181.

Newton, R. H., Haffegee, J. P. & Ho, M. W. 1995*a* Colour contrast in polarised light microscopy of weakly birefringent biological specimens. *J. Microsc.* **180**, 127.

Rusaouën, M., Pujol, J.-P., Bocquet, J., Veillard, A. & Borel, J. P. 1976 Evidence of collagen in the egg capsule of the dogfish *Scyliorhinus canicula*. *Comp. Biochem. Physiol.* B **53**, 539–543.

Vincent, J. G. V., Jeronimidis, G., Topping, B. H. V. & Khan, A. I. 1992 Biomimetics of flexible composites: Toward the development of new materials. *Biomimetics* **4**, 251–263.

Wourms, J. P. & Sheldon, H. 1972 Elasmobranch egg case formation: epithelial cell origin of collagen. *J. Cell Biol.* **55**, 290.

APPENDIX: MODELLING THE RETARDATION PRODUCED BY PARABOLIC ARRANGEMENTS OF FIBRILS

(*a*) *Transverse section of ribbon*

By reference to figures 32, the shape of the observed retardation plot along the x axis of the ribbon in a transverse section (figure 27*a* & *b*) can be related to a theoretical model derived from a parabolic function as follows.

Differentiating a parabolic function gives

$$dy/dx = -2Ax, \tag{1}$$

and leads to the following expression for σ, the angle of inclination of fibrils at any point:

$$\sigma = [\tan^{-1}(dy/dx)] \tag{2}$$

This enables L, the length of a tangent projected onto the image plane (figure 28) to be expressed as follows:

$$L = C \cos [\tan^{-1}(dy/dx)], \tag{3}$$

where C is a constant.

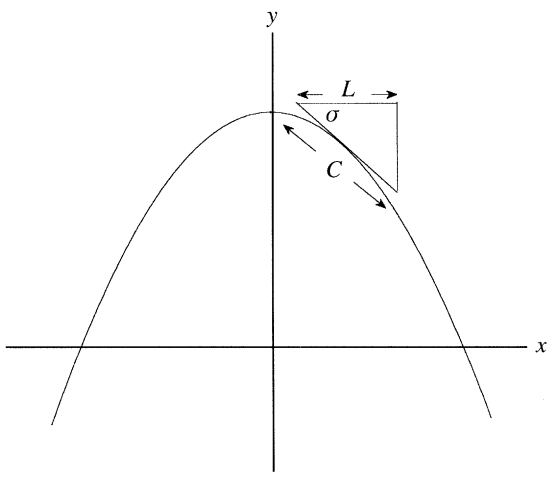

Figure 32. The relation between the slope of a parabola at any point and the length (L) proportional to retardation in a transverse section of the ribbon (see text).

Substituting (1) into (3)

$$L = C \cos [\tan^{-1}(-2Ax)]. \quad (4)$$

The retardation from the intrinsic birefringence will, at any x value in a transverse section, be proportional to L. The fact that there is very little matrix between the collagen fibrils in this system (see above and Knight & Feng 1994) suggests that the form birefringence is negligible and can be ignored. It therefore follows from (4) that total retardation (Λ) can be expressed

$$\Lambda = C_1 \cos [\tan^{-1}(-2Ax)] \quad (5)$$

From (5) when $x = 0$, $dy/dx = 0$, $\sigma = 0$

$$C_1 = \Lambda_{max}.$$

Substituting a typical observed value Λ_{max} into (4) gives

$$\Lambda = 27 \cos [\tan^{-1}(-Ax)].$$

The fit between the theoretical curve and the observed retardation plot is shown in figure 28*b* above.

(*b*) *Longitudinal section of ribbon*

Similarly, for a transect along the x axis of a longitudinally sectioned ribbon, it can be shown that

$$\Lambda = \tan^{-1}(dx/dy) \quad (6)$$

and that the total retardation (Λ) will be:

$$\Lambda = C_3 \cos [\tan^{-1}(+2Ax)] \quad (7)$$

where $C_3 = \Lambda_{min}$.

The similarity of the observed and predicted curves is shown in figures 27*b*,*c* and 29*b* above.

Received 16 November 1995; accepted 29 March 1996

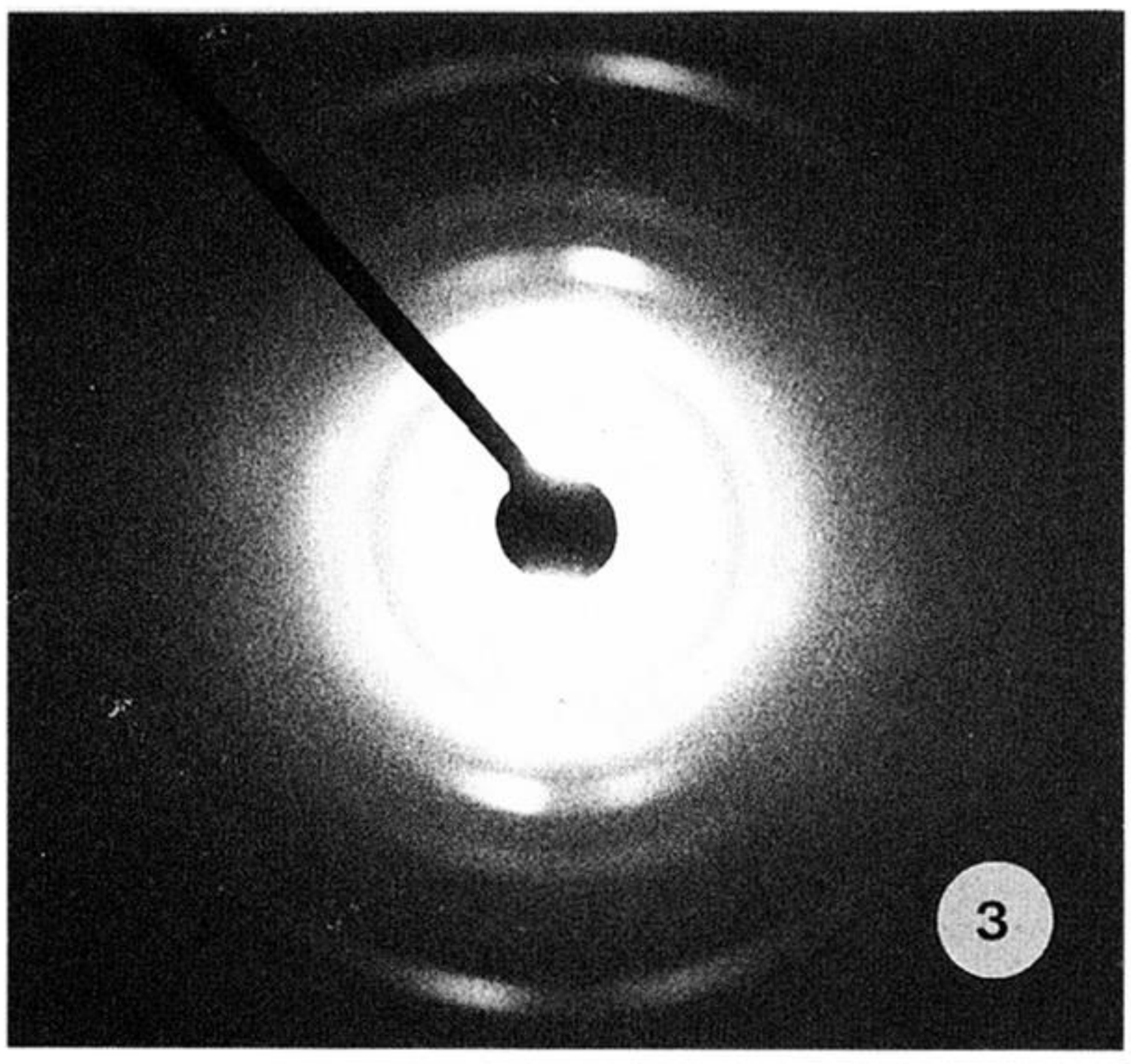

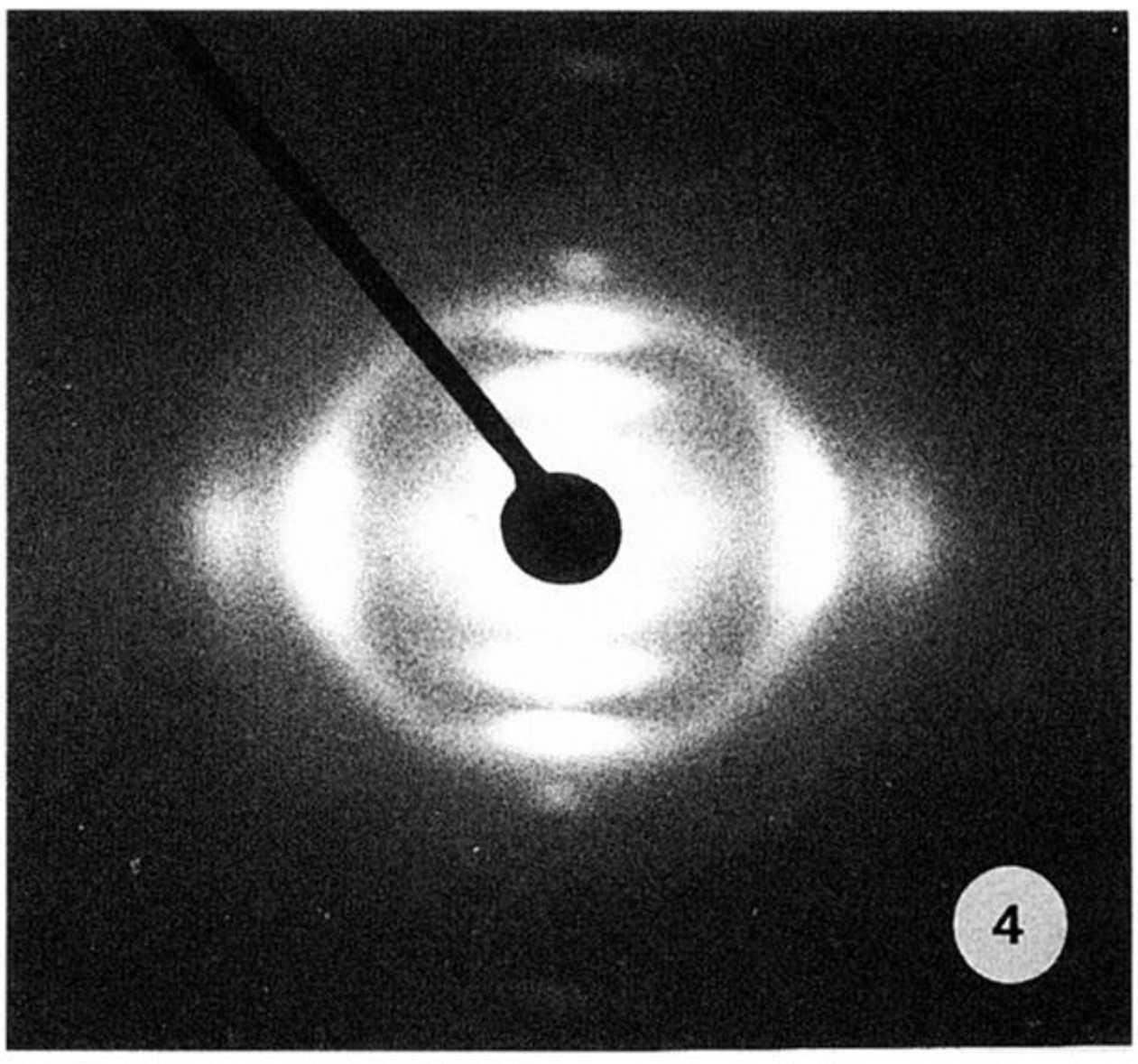

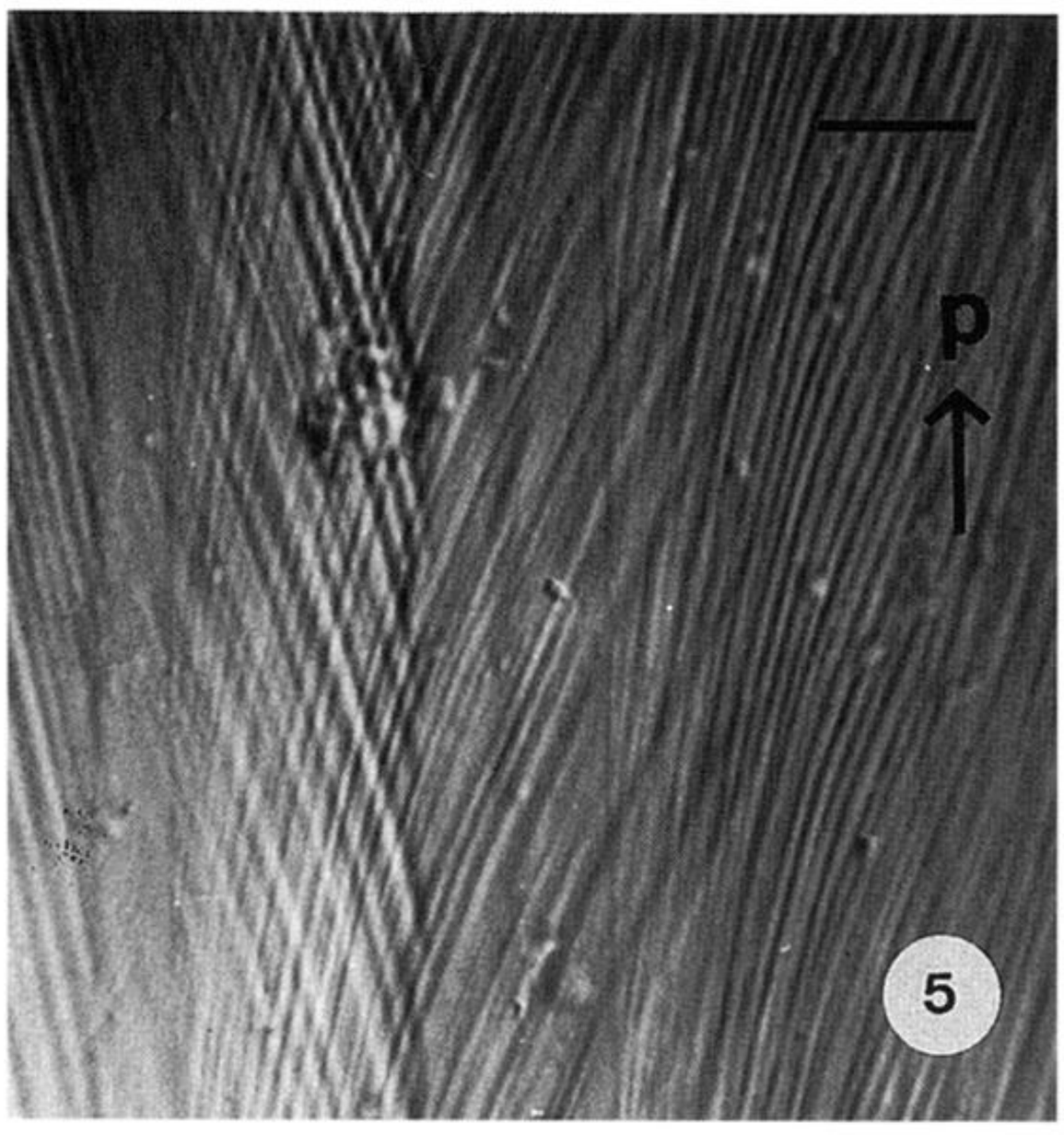

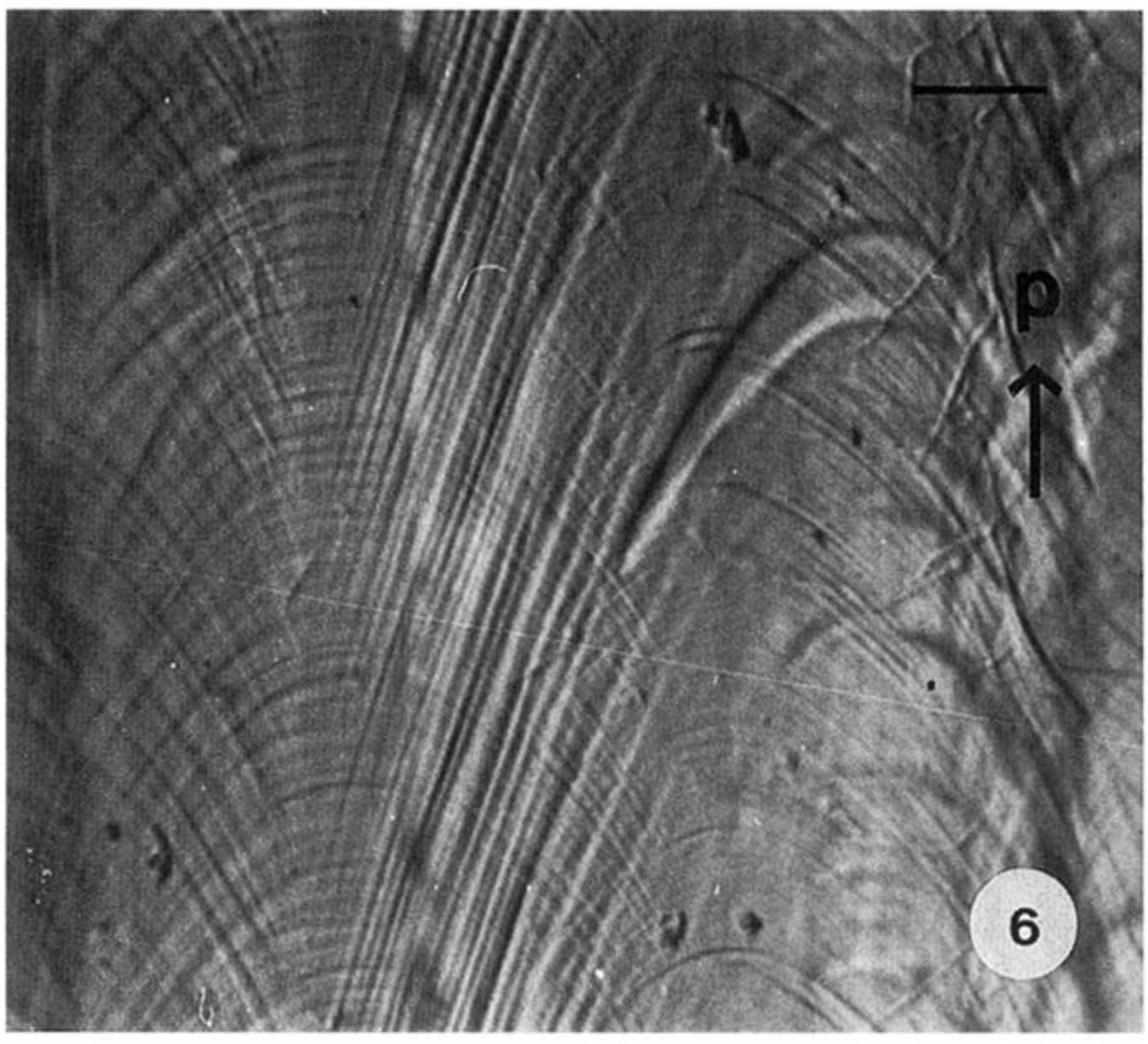

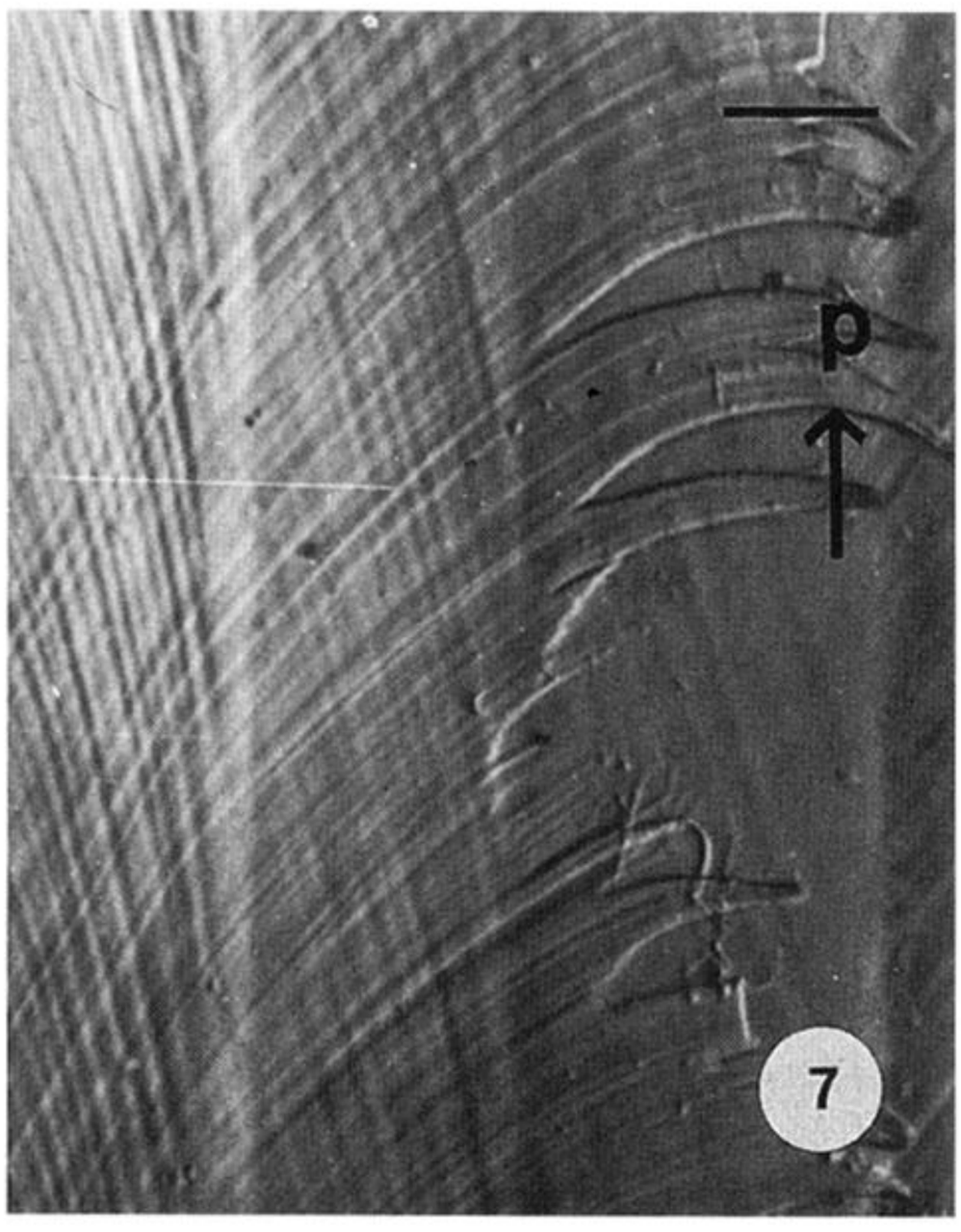

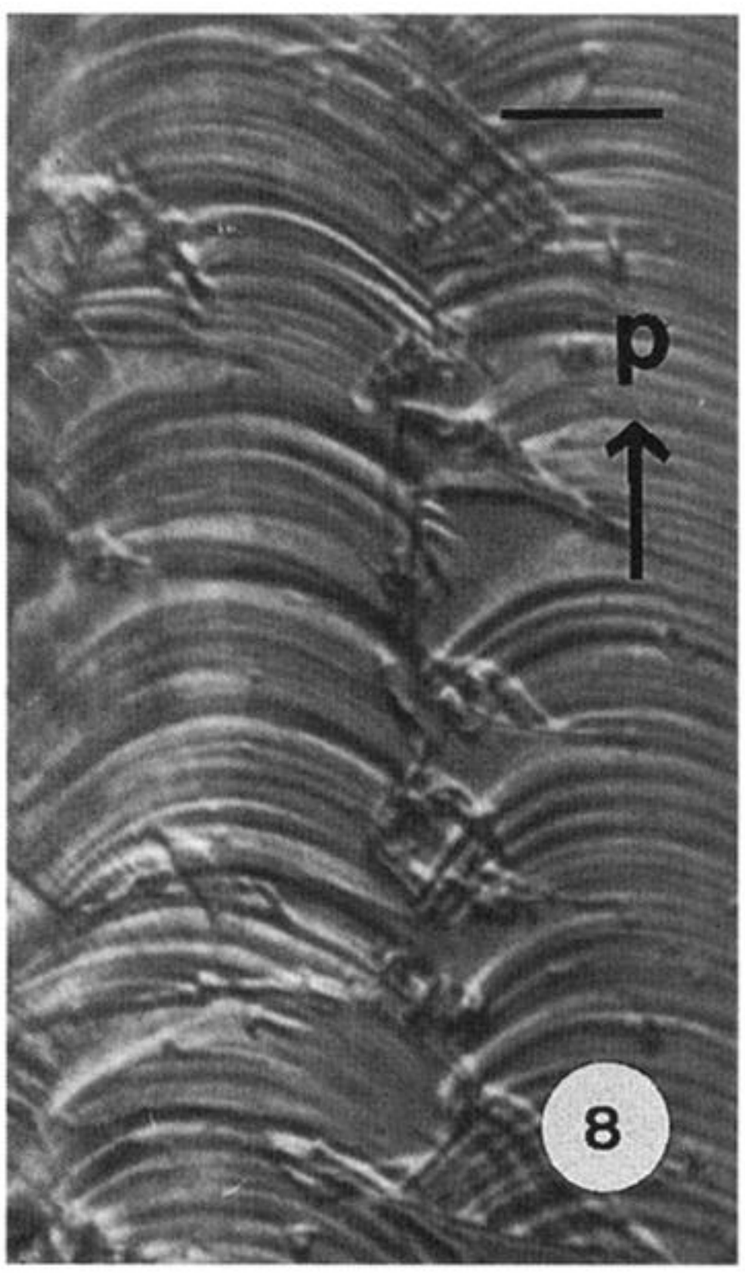

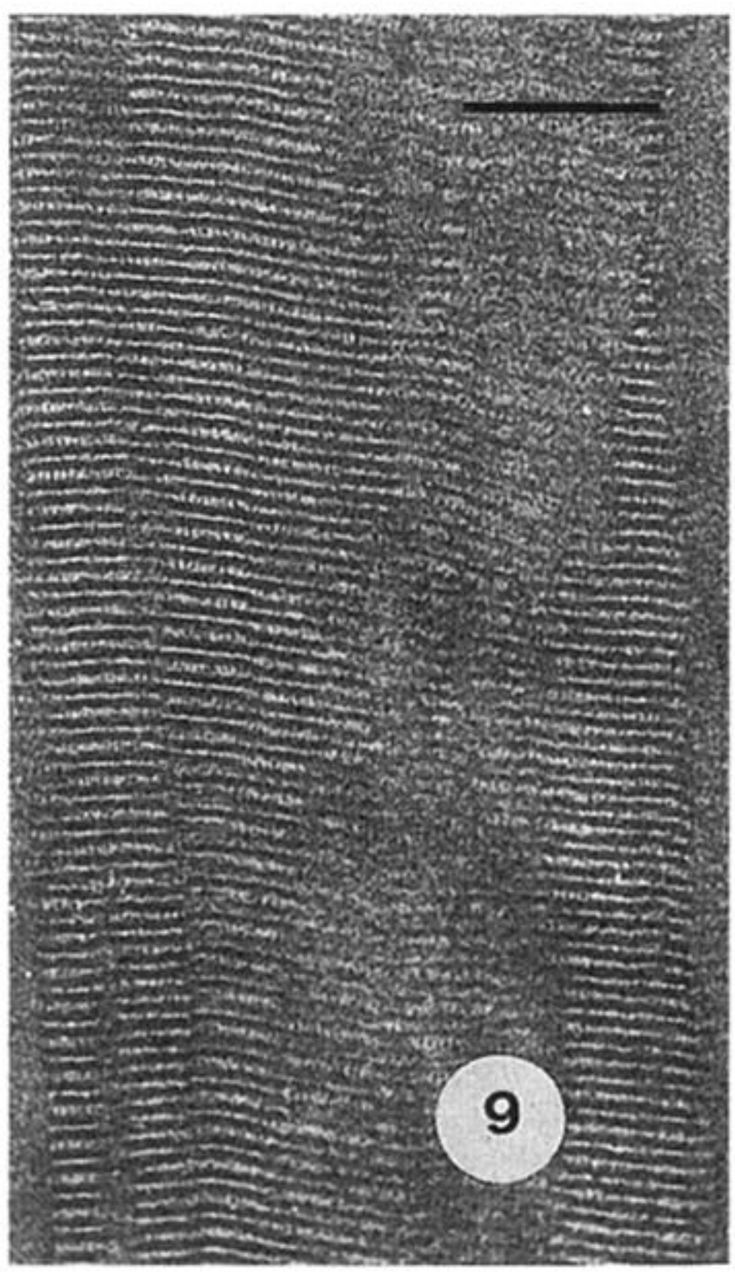

Figure 3. Low angle x-ray diffraction pattern recorded with the beam horizontal $\pm 2°$ (figure 1). See text.

Figure 4. As figure 2 but with the beam vertical $\pm 2°$. See text.

Figure 5. Nomarski micrograph of a peel from a region of the marginal rib close to the midline. The material has a fibrous texture with a predominantly biaxial pattern crossing at about 17°. Careful examination shows that the fibres appear curved. Posterior (p). Scale bar 20 μm.

Figure 6. As figure 5 but showing nested parabolic curves. Posterior (p). Scale bar 20 μm.

Figure 7. As figure 5 but showing splitting between the curved fibres at the torn edge of a ribbon to the right of the micrograph. The torn sheet is evidently quite thin. This pattern of splitting is unlikely in a twisted nematic construction. Posterior direction (p). Scale bar 20 μm.

Figure 8. As figure 5 but showing a pattern of slightly overlapping parabolic curves seen in lamellae stripped from the outer lamellae of L_2 of the capsule wall proper. The parabolae are more rounded than those seen in figure 6. Posterior (p). Scale bar 50 μm.

Figure 9. Transverse ultrathin section of part of the central portion of a ribbon showing a number of fibrils running north/south across the micrograph and parallel to the *x* axis of the ribbon. The banding pattern appears closely similar to that of fibrils from the capsule wall proper and is in accurate lateral registration for much of the thickness of the bundle. Scale bar 200 nm.

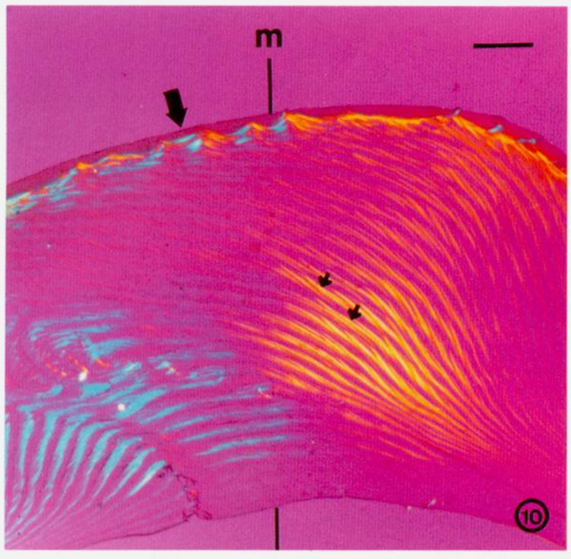

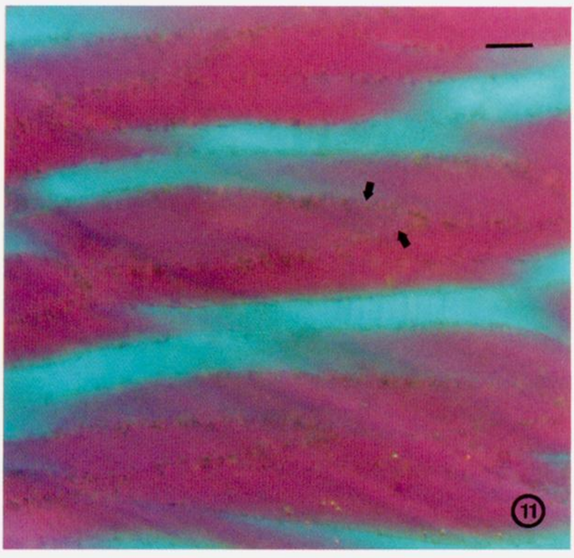

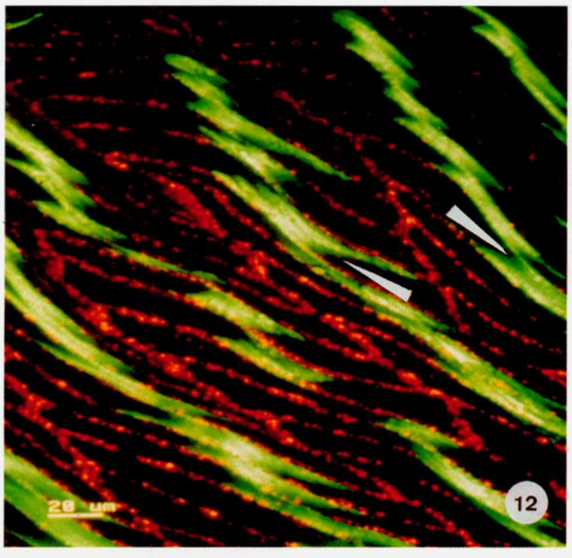

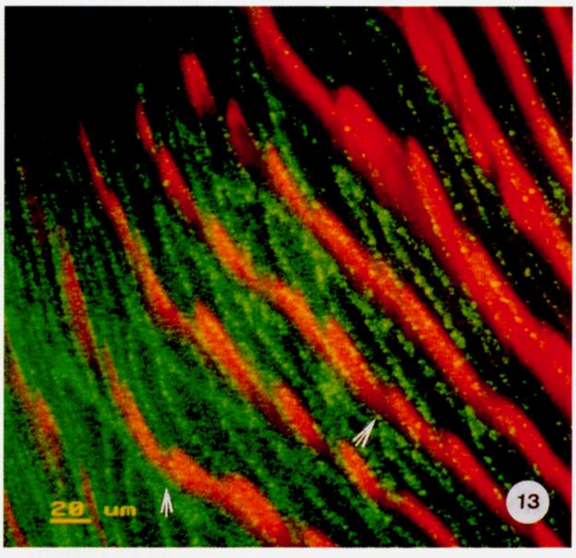

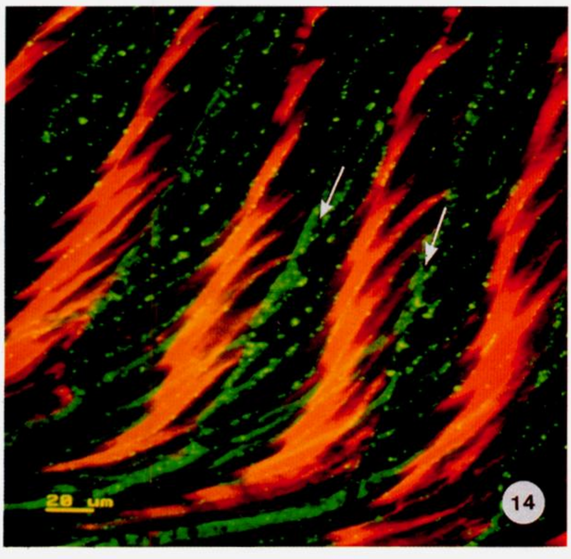

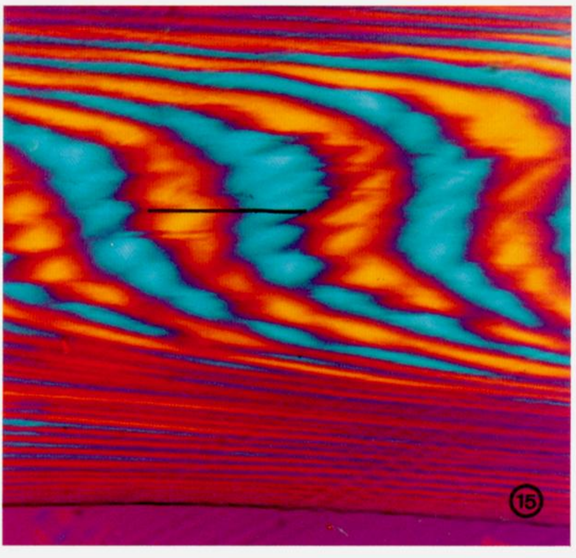

Figure 10. Polarizing micrograph of a transverse cryostat section of part of the marginal rib. The slow axis of the analyser ran from left to right. The first order red plate was set at an angle of 7.5° to this. The lamellae (narrow arrows) of layer L_2 are somewhat curved and can be seen to be constructed from rows of partly overlapping ribbons, the central parts of which are brightly and positively birefringent (blue interference colours to left and yellow to right of micrograph). Midline of the rib (m); outer surface (broad arrow). The outlines of the ribbons are not clearly demarcated in this figure. There approximate positions can be identified by reference to figure 12. Scale bar 200 µm.

Figure 11. As figure 10 but at a greater magnification. The slow axis of the polarizer lay at −45° to the left to right axis of the figure. The ribbon can be seen to be outlined by tiny highly refractile granules (arrows). Only the central part of the ribbon (blue) appears strongly birefringent. This is because the *y* axis of the parabolae lie normal to the plane of section so that only fibrils at their apices lie parallel to the plane of section. Scale bar 10 µm

Figure 12. Cryostat section cut at 90° to the long axis of the marginal rib in a region similar to that appearing yellow in figure 10. Confocal autofluorescent image superimposed on non-confocal birefringent image; computer generated false colours. The slow axis of the analyser runs from left to right. The granular material outlining the ribbon (see figure 11) is autofluorescent (orange). The central part of each ribbon, representing the apex of the parabolic fibres, is positively birefringent (green or white depending on strength) and shows a fibrous texture in places (arrows). There is a sharp line demarcating the edge of the strongly birefringent portion and this is frequently parallel to the ends of the ribbon (see top third of micrograph). This observation is compatible with the staggered model shown in figure 25. Scale bar 20 µm

Figure 13. As figure 12 but cryostat section cut at approximately 75° to the long axis. Autofluorescence (green); birefringence (orange). Compared with figure 12, tilting the plane of sectioning has, as predicted, shifted the birefringent region to the end of each ribbon (arrows). Scale bar 20 µm

Figure 14. As figure 12 but cryostat section cut at approximately 85° to the long axis of the marginal rib and close to the edge of the autofluorescent area. Fluorescence (green); birefringence (orange). The ends of the ribbons (arrows) define the plane of the lamella. Material at the edge of the lamella lay adjacent to the wall of the transverse groove in the spinneret while material on the long faces of the ribbon lay adjacent to the baffle plates. This suggests that the fluorescent material is applied to the forming ribbon in or just before the spinneret. Scale bar 20 µm

Figure 15. Polarizing micrograph as figure 10 but section cut at approximately 15° to the long axis of the marginal rib. The upper edge of the section shows an alternation of thin, parallel laminae with molecules at +45° (blue), 0° (magenta), −45° (yellow) and 0° (magenta) as in a longitudinal section. Beneath this, curvature of the planes of the lamellae greatly broadens the pattern. Here the alternation in orientations can be clearly seen. Results from a transect along a line similar to that indicated are illustrated in figure 27. Transect line 400 µm

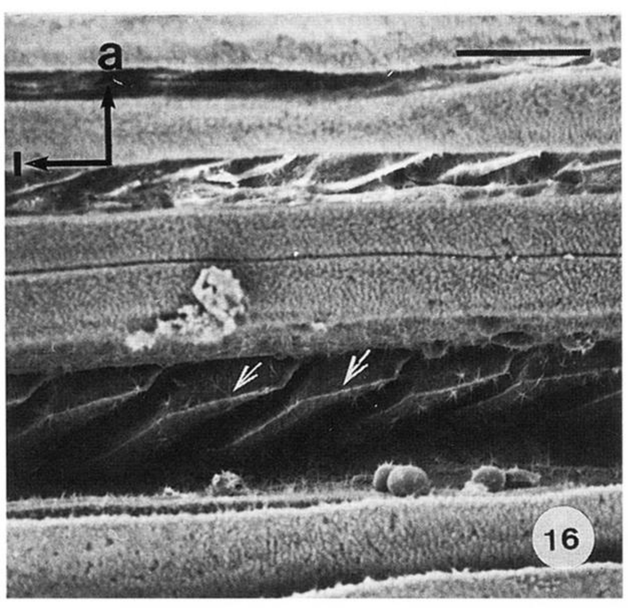

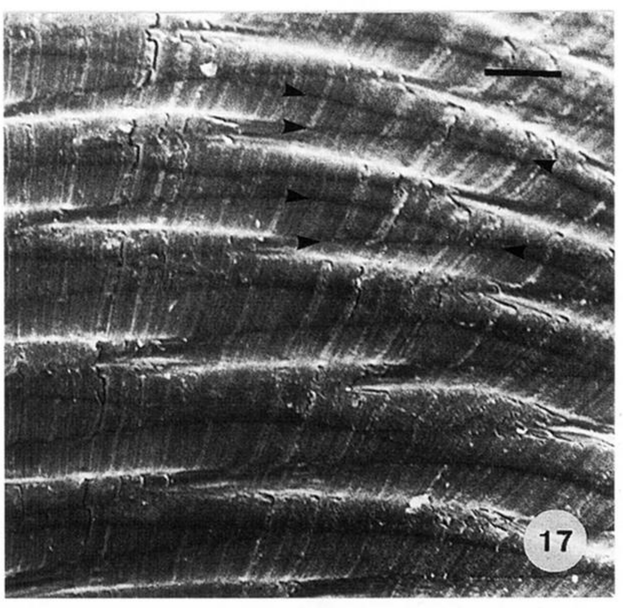

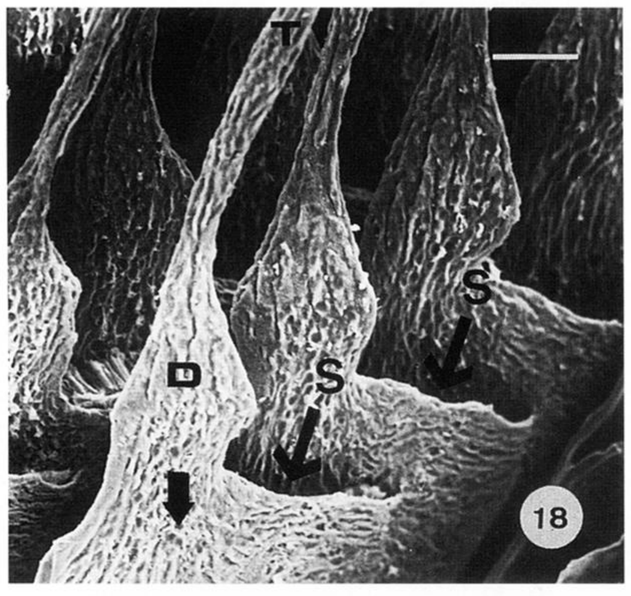

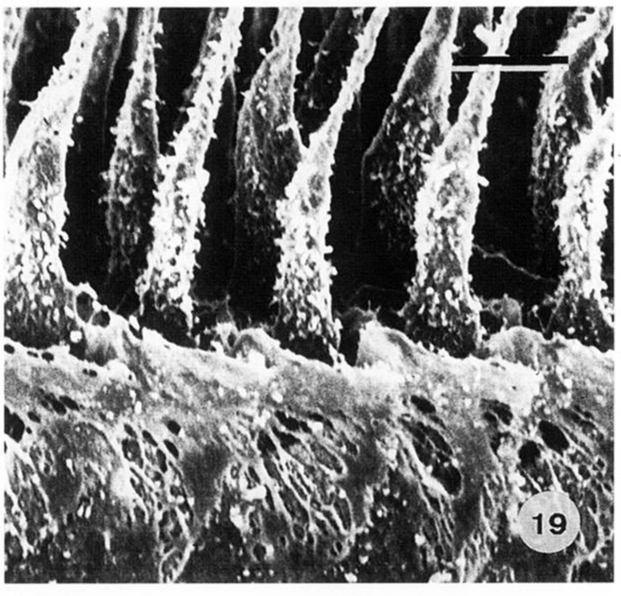

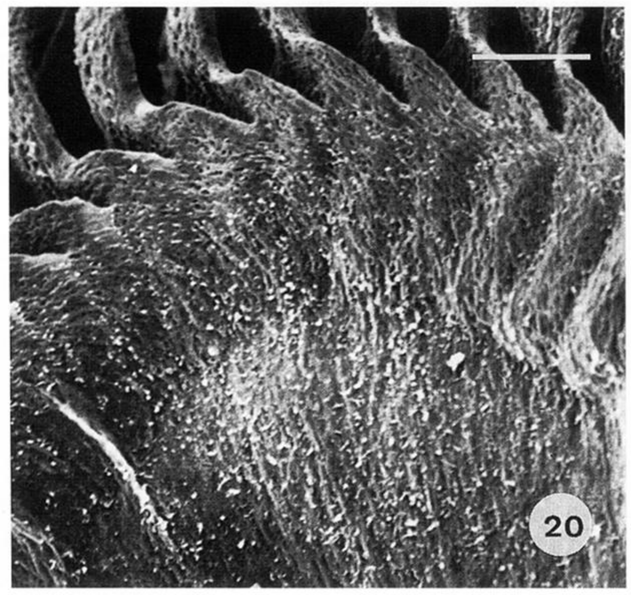

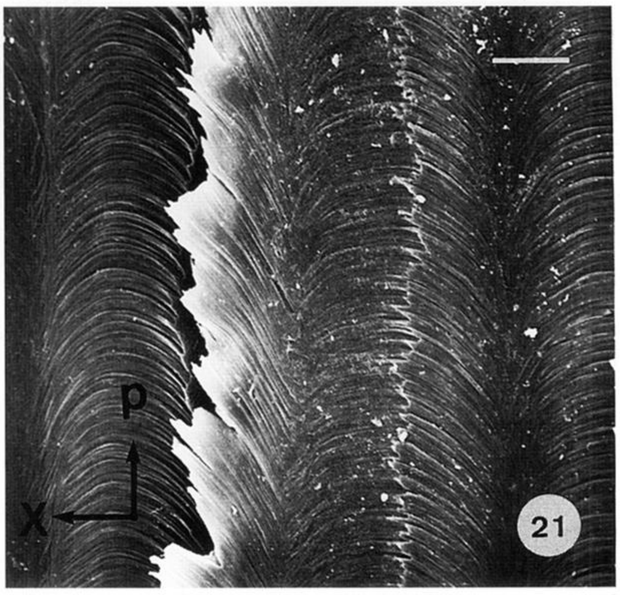

Figure 16. SEM looking down parts of two transverse grooves (running left to right) in the region of the nidamental gland which secretes the layer L_2 of the capsule wall proper. The baffle plates (arrowed) of the spinnerets can be seen overlapping and inclined at an angle of about 30° to the long axis of the groove. Compare with figure 17. Anterior (a); lateral (l). Scale bar 100 μm

Figure 17. SEM of the cut surface of a transversely sectioned marginal rib. The similarity of the shape, size and orientation of the ribbons to the spinnerets which form them (figure 16) is remarkable. The ribbons appear outlined by a dark line (arrows) probably representing the autofluorescent material (compare with figures 12–14). The systematic changes in thickness probably represent an artefact caused by sectioning fibrils at different orientations. Scale bar 40 μm

Figure 18. SEM of a natural cast (see text) of spinnerets from the tendril/marginal rib forming region viewed from the posterior side. Secreted material is thought to flow down the lumen of the gland tubule (T) in a liquid crystalline state to pass through the secretory duct (D) into the space (S) between the baffle plates whose former position is indicated (arrow). The baffle plates were usually lost as the secreted material was pulled from the gland during specimen preparation. The surface of the material has a fibrous texture at right angles to the orientation of the collagen molecules within the material. Scale bar 50 μm

Figure 19. As figure 18. The development of a curving pattern of fibres (arrows) can be seen as the secreted material flows on further between the baffle plates. Posterior (P); Lateral (L). Scale bar 100 μm

Figure 20. As figure 18. The development of the curving pattern can be traced as the material flows on further apically through the transverse groove. The orientation of the material close to the wall of the transverse groove appears to be to be predominantly longitudinal. Scale bar 100 μm

Figure 21. SEM of peel preparation. The parabolic curves appear to be generated from curved fibres (arrows). Approximately half of a thin sheet appears to have been torn away from the central ribbon. This indicates that the ribbon is constructed from several layers of thin sheets laid on one another. In this case the parabolae in successive sheets appear to share the same y axis. Posterior (p); x axis of the ribbon (X). Scale bar 20 μm

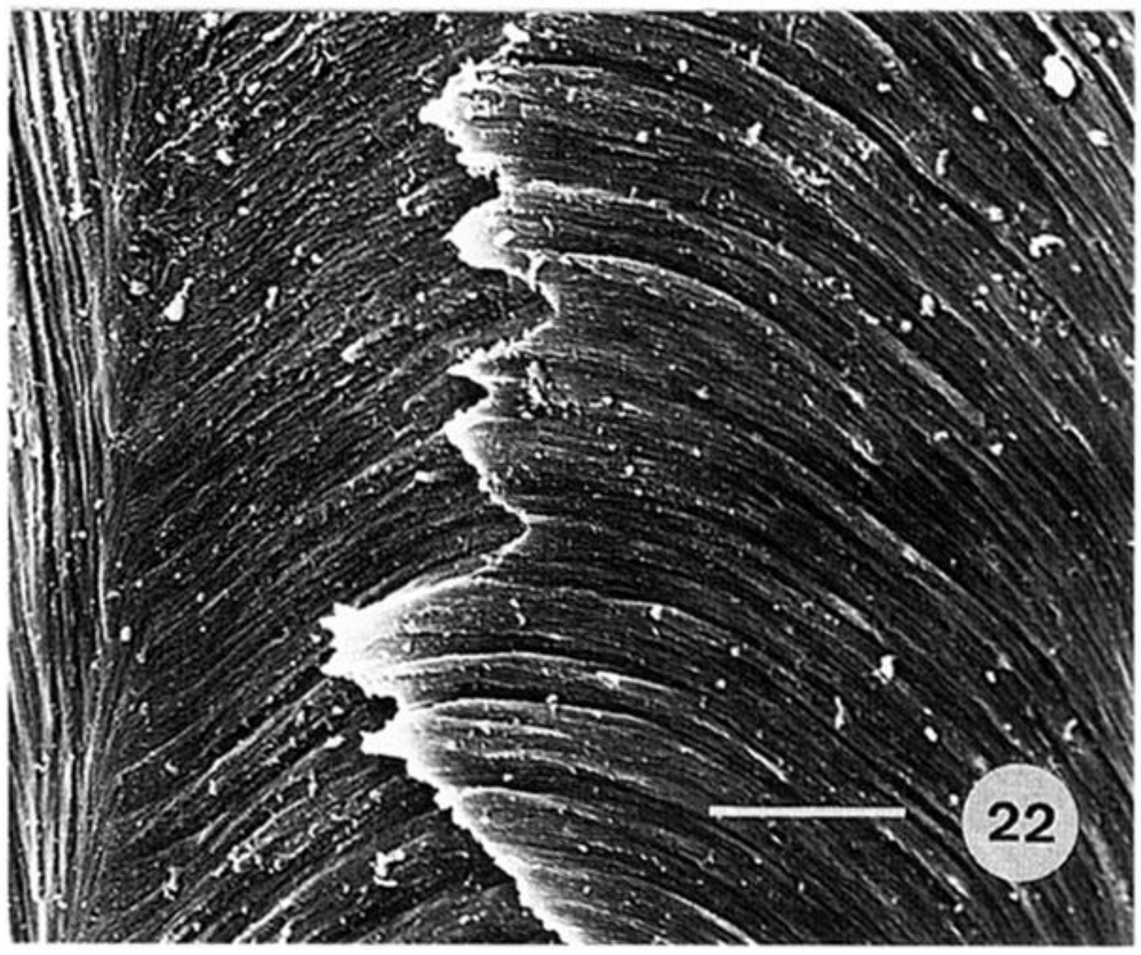

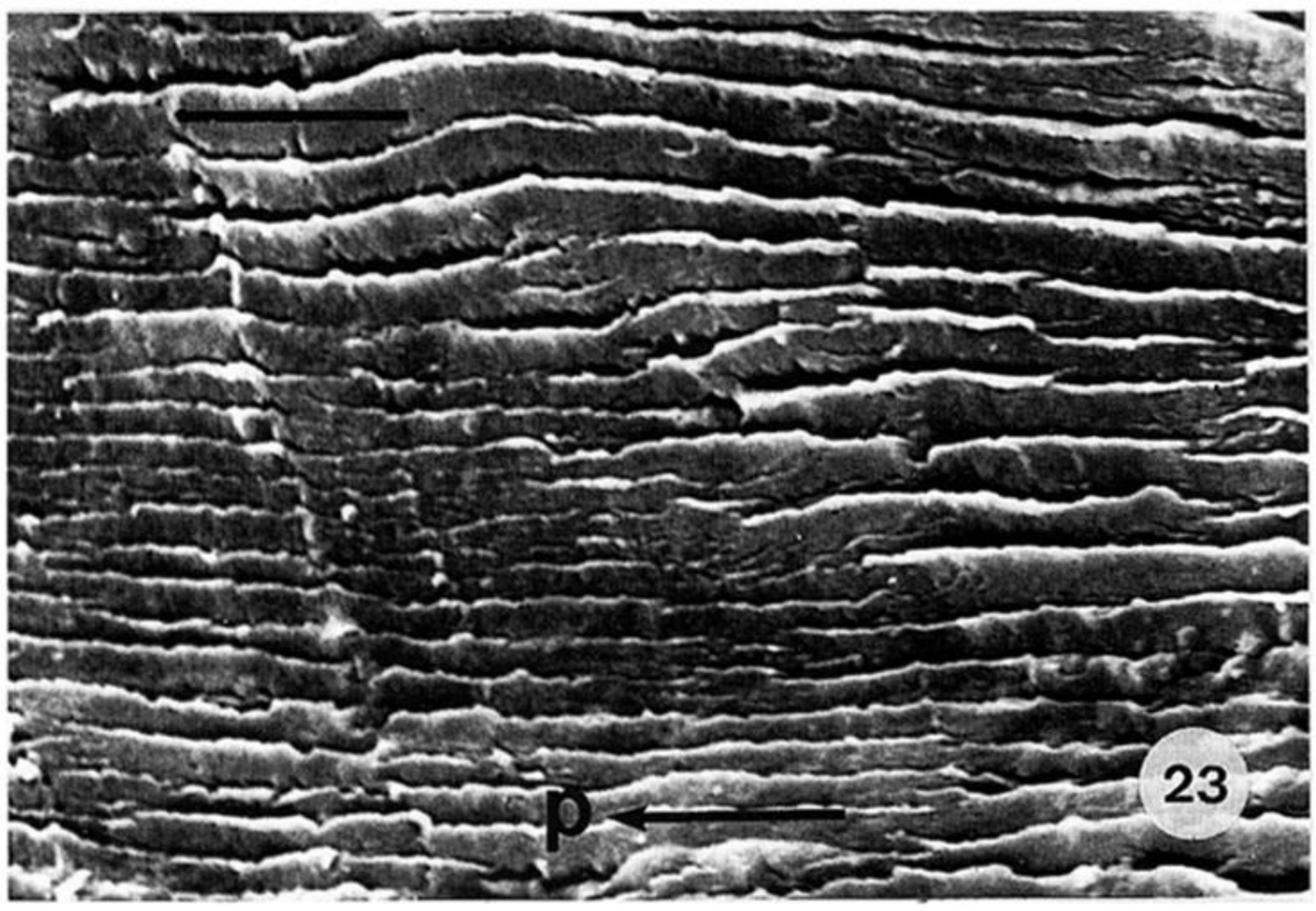

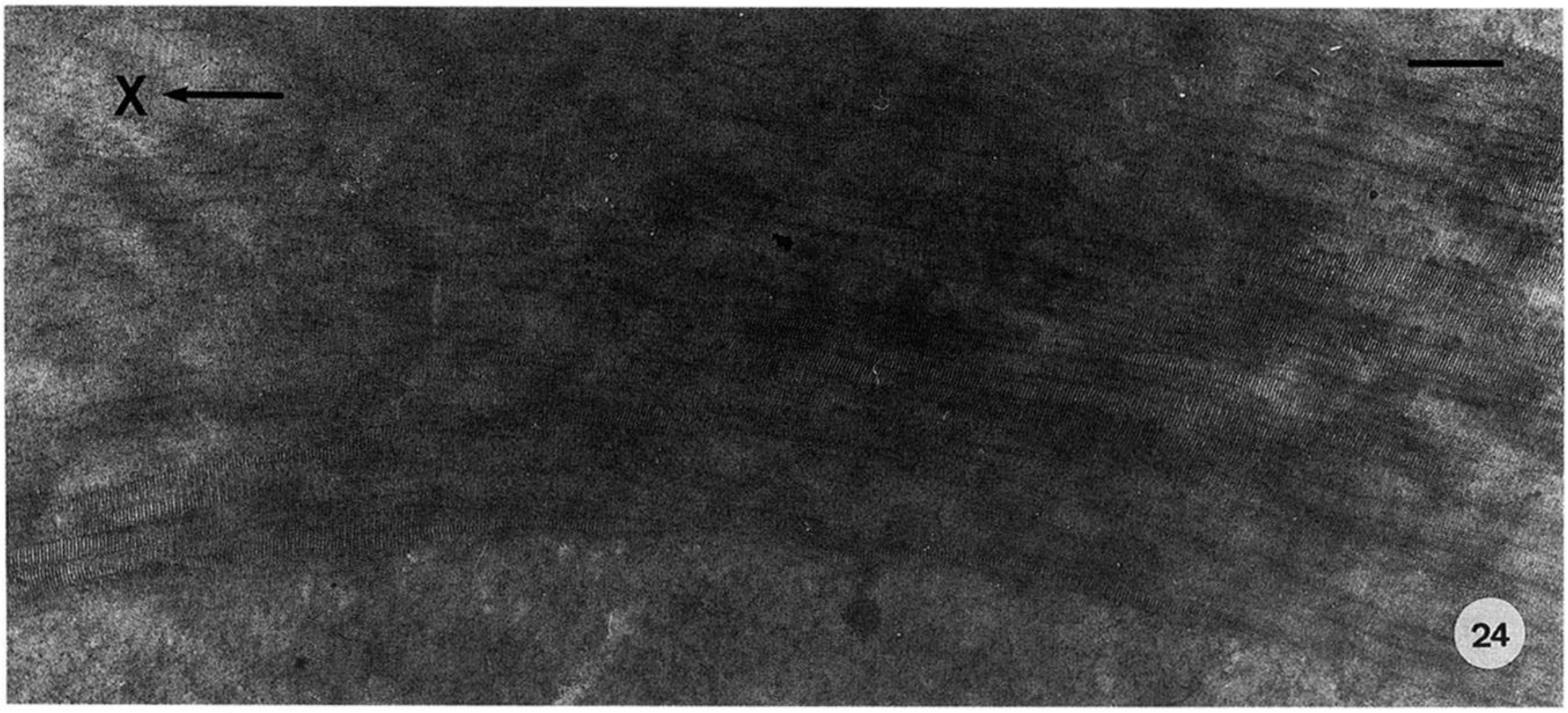

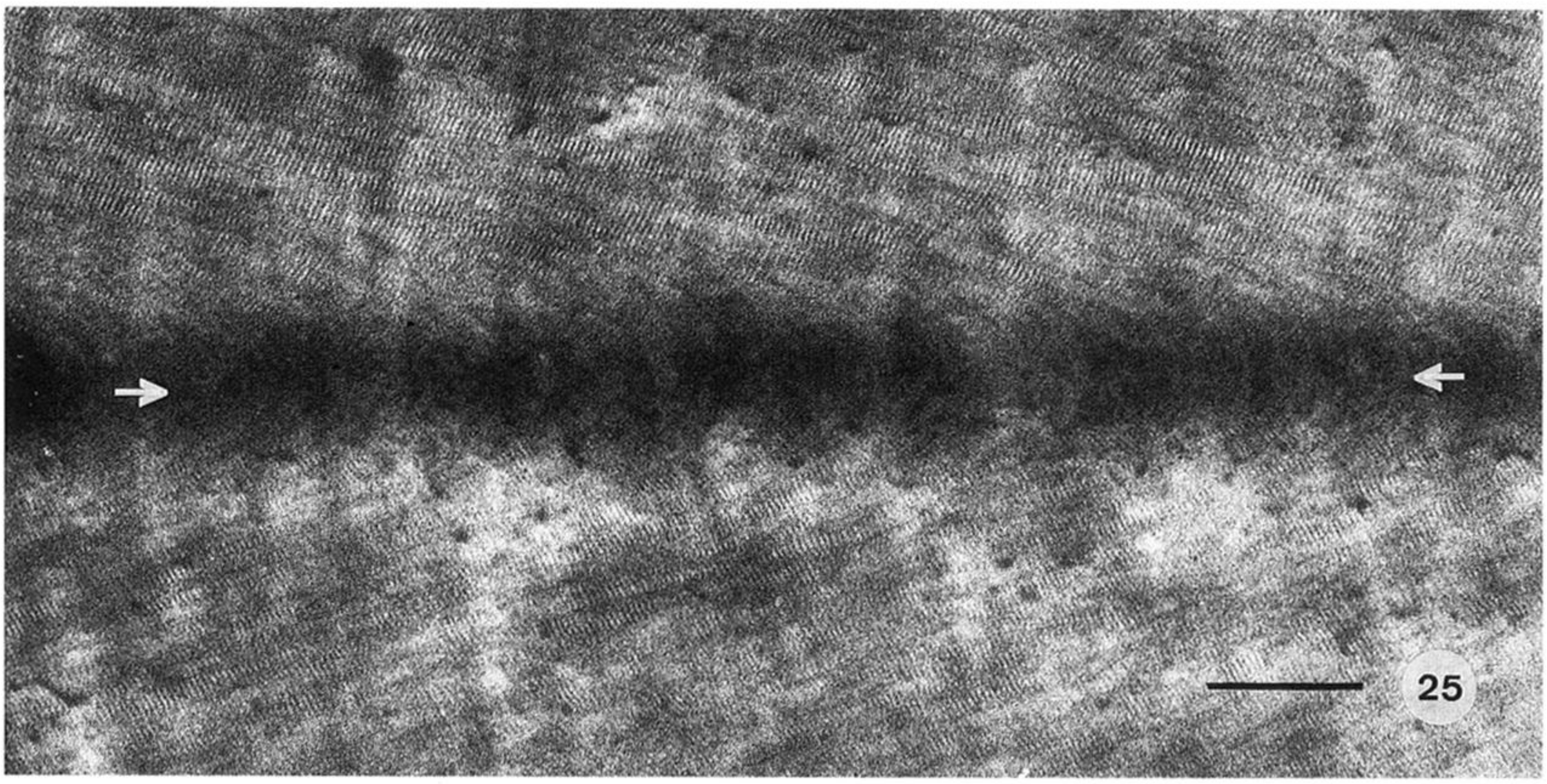

Figure 22. As figure 21. The ribbon can be clearly seen to be constructed from curved fibres laid in thin parallel sheets. The *y* axis of the parabolae appears to be slightly staggered in the two successive sheets. Scale bar 5 μm

Figure 23. SEM of part of a ribbon which appears to have fractured approximately longitudinally and approximately at right angles to the *x* axis. The ribbon appears to be constructed from numerous thin sheets. anteroposterior axis (p). Scale bar 4 μm

Figure 24. TEM showing the central part of a ribbon seen in a transverse ultrathin section. The orientation of the fibrils here confirms the polarizing microscope observations. Successive collagen fibrils appear to rotate in the **x** plane (X) arrows. There is some evidence of a successive staggering of regions showing accurately longitudinally sectioned fibrils (see also figures 12, 22 and 26). Scale bar 500 nm

Figure 25. TEM of ultrathin HLS showing the rapid rotation of fibrils at the junction between two ribbons which appears as a dark line (arrows). The apogee of the tight parabolae formed in this way point anteriorly, in the opposite direction to the broader parabolae in the middle of the ribbon not seen in this figure. Scale bar 500 nm